

Photon sphere and quasinormal modes in AdS/CFT

Koji Hashimoto, Kakeru Sugiura, Katsuyuki Sugiyama, Takuya Yoda

Department of Physics, Kyoto University, Sakyo-ku, Kyoto 606-8502, Japan

E-mail: koji@scphys.kyoto-u.ac.jp,

sugiura@gauge.scphys.kyoto-u.ac.jp, sugiyama@scphys.kyoto-u.ac.jp,

t.yoda@gauge.scphys.kyoto-u.ac.jp

ABSTRACT: Photon spheres are the characteristic of general black holes, thus are a suitable touchstone for the emergence of gravitational spacetime in the AdS/CFT correspondence. We provide a spectral analysis of an AdS Schwarzschild black hole near its photon sphere. We find that quasinormal modes near the photon sphere reflect the AdS boundary, resulting in a peculiar spectral pattern. Our large angular momentum analysis owes to an analogue to solvable Schrödinger equations such as an inverted harmonic oscillator and the Pöschl-Teller model, with a Dirichlet boundary condition. Through the AdS/CFT dictionary, it predicts the existence of a peculiar subsector in the large angular momentum spectrum of thermal holographic CFTs on a sphere.

Contents

1	Introduction	1
2	Photon sphere in AdS black hole	3
3	From quasinormal modes to quantum mechanics	6
3.1	Potential hill relates to the quantum-mechanical model	6
3.2	Large l expansion	7
3.2.1	Quasinormal modes and quantum mechanical spectrum	7
3.2.2	On the validity of inverted harmonic oscillator	8
3.2.3	AdS boundary is a hard wall	9
3.3	Analytic potential at high temperature	9
4	Solving quasinormal modes respecting AdS boundary	11
4.1	Inverted harmonic oscillator	11
4.2	Pöschl-Teller model	14
5	Summary and discussion	18
A	Representation of $SL(2; \mathbf{R})$	20
A.1	Relation between $SO(2, 1)$, $SU(1, 1)$ and $SL(2; \mathbf{R})$	20
A.2	Representation of $su(1, 1)$	22
B	Solvable models and symmetry	25
B.1	Inverted harmonic oscillator	25
B.1.1	$SL(2; \mathbf{R})$ symmetry and spectra	25
B.1.2	Wave functions and spectra	28
B.2	Pöschl-Teller model	31
B.2.1	Wave functions and spectra	31
B.2.2	$SL(2; \mathbf{R})$ symmetry and spectra	34

1 Introduction

Since the whole mechanism of the holographic principle has not yet uncovered, any possible indicator of the emergence of a gravitational spacetime is welcome to be tested in the dictionary of the AdS/CFT correspondence [1]. As is popularly known, *photon spheres* are the characteristic of general black holes, needless to speak about the recent observation of an Einstein ring in the M87 black hole [2]. Therefore it is natural to study the photon spheres in the context of the AdS/CFT, to find whether the photon spheres can be an indicator of the spacetime emergence, from the viewpoint of the dual CFT.

The photon spheres are best-understood in a particle picture as its eternal motion circulating the black hole. In general, for spherical black holes, the photon sphere is a sphere on which photons can circulate the black hole forever. The orbit is unstable: the circulating photon can be swallowed by the black hole or escape from it, once perturbed infinitesimally. The effective motion is dictated by the null geodesics determined by the effective potential which has a peak at the photon sphere. This potential hill is made just by the combination of the gravitational attraction and the centrifugal force of the angular momentum of the photon.

The fundamental relation in the AdS/CFT dictionary is the coincidence of the spectra in the gravity side and the CFT side. In the gravity side, the spectrum is nothing but the quasinormal modes (QNMs): the fluctuation spectrum of (photon) fields in the background of a black hole. The field, once quantized, should correspond to a particle orbiting the black hole. Therefore in general the spectra of the QNMs should also be affected by the photon sphere.

For our study of the photon sphere in the AdS/CFT, we find three important streams of research development. First, recently, it was shown that a symmetry group $SL(2; \mathbf{R})$ dictates the QNM spectra near the photon sphere/ring of Schwarzschild and Kerr black holes in an asymptotically flat spacetime [3, 4]. The analysis was further generalized to warped geometries [5, 6] and related properties were studied [7, 8]. On the other hand, the QNMs in the AdS Schwarzschild black hole has a long history: they were first studied in [9–11], and the general study in the WKB approximation was performed by Festuccia and Liu in [12] (see also [13–31] for various QNM analyses in AdS black holes, and see [32, 33] for reviews). Thirdly, the direct consequence of the existence of the photon sphere is the Einstein ring in images of general black holes, and an imaging transform on holographic CFTs indeed was shown to produce such Einstein rings [34, 35].

In this paper, motivated by these works, we study QNMs near the photon sphere in the AdS Schwarzschild black hole. We find a peculiar form of the spectra associated with the photon sphere. Through the AdS/CFT, this shows the existence of a peculiar subsector in the large angular momentum spectrum of thermal holographic CFTs on a sphere at high temperature.

We first look at the existence condition of the photon sphere in the AdS Schwarzschild geometry. In fact, there exists a minimum angular momentum for the existence of the potential hill [12]. We estimate the minimum to find typical values of the angular momentum which we focus on.

To obtain the QNM spectrum of our concern, we map the wave equation for the QNMs to a Schrödinger equation with a potential hill. The photon sphere is located at the top of the Schrödinger potential hill around which the potential can be approximated by an inverted harmonic oscillator. At a large angular momentum, the approximation is better, as expected from the results reported in the asymptotically flat case [4]. We find that a large angular momentum limit brings the quantum mechanics to a simple form: a potential hill at the photon sphere, and a Dirichlet boundary at the asymptotic AdS infinity. We obtain an explicit relation between the CFT spectrum and the energy spectrum of the Schrödinger equation. At high temperature, we find an analytic expression for the Schrödinger potential.

The Schrödinger equation is not integrable, thus to grasp a possible universal feature of the energy spectra, we resort to solvable quantum mechanics which share the feature of our Schrödinger equation. In fact, the solvable models have been used in the analyses of QNMs [36], and presently can provide an analytic expression for the energy spectrum. We use an inverted harmonic oscillator and the Pöschl-Teller model, both of which have the potential hill.

In solving those, we find that the existence of the AdS boundary is essential. Even when we bring the AdS boundary to the spatial infinity effectively (which is possible by taking the large angular momentum limit), the effect of the boundary still remains crucial, and the spectrum does not lead to that of the asymptotically flat case.

As these two solvable models provide a spectral pattern similar to each other, we claim that our system of the QNMs near the photon sphere in the AdS Schwarzschild black hole should share the pattern. Through the AdS/CFT dictionary, the obtained spectrum corresponds to the spectrum of a peculiar subsector of the thermal CFT on a sphere.

The organization of this paper is as follows. In Sec. 2, we examine the existence condition of the photon sphere in the AdS Schwarzschild. Then in Sec. 3, we relate the QNM equation with a Schrödinger equation of a quantum mechanics with a potential hill, and find an explicit relation between the QNM spectrum at a large angular momentum and the quantum mechanical energy. In Sec. 4, we solve the spectrum of solvable quantum models analogous to the one given in Sec. 3, and obtain the pattern of the QNM spectrum. Sec. 5 is for our summary and discussions. In App. A we summarize the representation theory of $SL(2; \mathbf{R})$, to illustrate that it is broken by the AdS boundary. App. B is for detailed information on the solvable models used in Sec. 4.

2 Photon sphere in AdS black hole

In this section, the photon sphere in the AdS Schwarzschild black hole spacetime is described. We demonstrate that a test field feels a photon sphere for any Hawking temperature T , taking a sufficiently large angular momentum $l > l_{\min}$, where l_{\min} is a T -dependent minimum. Then, the T -dependence of l_{\min} is estimated.

In the cases in the ordinary Schwarzschild black hole, nonzero angular momentum always produces a photon sphere. In the asymptotic AdS cases, however, the centrifugal potential is buried by the AdS curvature and the photon sphere disappears for small l .

Let us consider a scalar field Φ with mass μ in the d -dimensional AdS Schwarzschild spacetime

$$ds^2 = -f(r)dt^2 + \frac{dr^2}{f(r)} + r^2 d\Omega_{d-2}^2, \quad f(r) = 1 + \frac{r^2}{l_0^2} - \left(\frac{r_0}{r}\right)^{d-3}, \quad (2.1)$$

where $d \geq 4$, l_0 is the AdS radius, and r_0 corresponds to the black hole temperature T .¹

¹The horizon radius r_h is related to this parameter r_0 as $r_0 = r_h(1 + r_h^2/l_0^2)^{1/(d-3)}$. This is a monotonic function of r_h . The black hole temperature T , which is equal to the dual CFT temperature, is given by $T = ((d-1)(r_h/l_0)^2 + (d-3))/4\pi r_h$. At high temperature (large black holes, $r_h \gg l_0$), we find $T \sim (d-1)r_h/4\pi l_0^2$ and $r_0 \sim r_h(r_h/l_0)^{2/(d-3)}$, thus $r_0 \sim l_0(4\pi l_0 T/(d-1))^{(d-1)/(d-3)}$. This means that the parameter r_0 is a monotonic function of T , at high temperature.

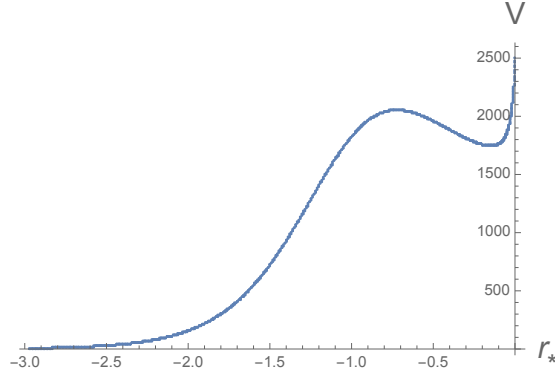


Figure 1. The effective potential V in the tortoise coordinate r_* . The peaks near $r_* = -0.6$ and $r_* = 0$ represent the photon sphere and the AdS boundary, respectively. For this figure we took $d = 4$, $r_0/l_0 = 4\sqrt{3}/9$, and $l = 40$.

Decomposing the scalar field to the spherical harmonics as $\Phi = e^{-i\Omega t} Y_{lm}(\text{angles}) \psi(r) r^{1-d/2}$, the Klein-Gordon equation reduces to a Schrödinger-like equation [37]

$$\left(\frac{d^2}{dr_*^2} + \Omega^2 - V(r) \right) \psi(r) = 0, \quad (2.2)$$

where

$$r_* \equiv \int_{\infty}^r \frac{dr'}{f(r')} \quad (2.3)$$

is the tortoise coordinate (the AdS boundary is at $r_* = 0$) and V is the effective potential defined by

$$V(r) = f \left(\frac{(l + d/2 - 1)(l + d/2 - 2)}{r^2} + \left(\frac{d}{2} - 1 \right) \left(\frac{d}{2} - 2 \right) \frac{f - 1}{r^2} + \left(\frac{d}{2} - 1 \right) \frac{f'}{r} + \mu^2 \right). \quad (2.4)$$

The potential in the tortoise coordinate r_* is illustrated in Fig. 1.

The potential (2.4) is found to be a sum of the potential in the flat case and corrections to it:

$$V(r) = \left(1 - \left(\frac{r_0}{r} \right)^{d-3} \right) \left(\frac{(l + d/2 - 1)(l + d/2 - 2)}{r^2} + \left(\frac{d}{2} - 1 \right)^2 \frac{r_0^{d-3}}{r^{d-1}} + \mu_{\text{eff}}^2 \right) + \frac{1}{l_0^2} \left(\mu_{\text{eff}}^2 r^2 + \left(\frac{d}{2} - 1 \right)^2 \left(\frac{r_0}{r} \right)^{d-3} + \left(l + \frac{d}{2} - 1 \right) \left(l + \frac{d}{2} - 2 \right) \right). \quad (2.5)$$

The effect of the AdS curvature consists of 1) the effective mass $\mu_{\text{eff}}^2 = \mu^2 + d(d-2)/4l_0^2$, 2) the r^2 term typical of AdS, and 3) the additional attractive term from the black hole; all of these tend to make the photon sphere vanish.

If l is large enough, the effective potential (2.4) of the scalar field reduces to the potential of the massless geodesic

$$V(r) \approx f(r) \frac{l^2}{r^2}. \quad (2.6)$$

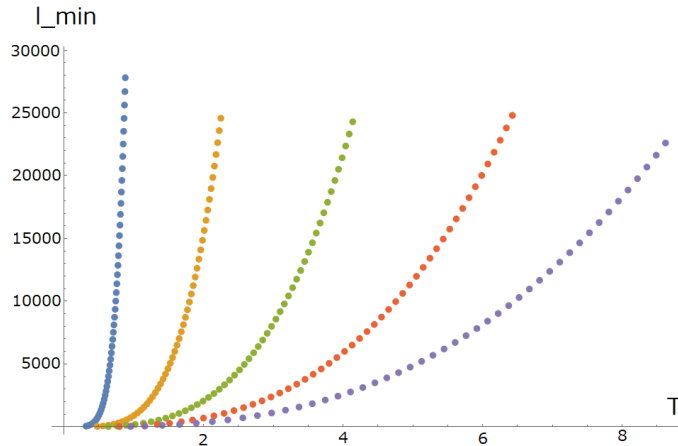


Figure 2. The T -dependence of the minimum angular momenta l_{\min} to generate a photon sphere in various spacetime dimensions d . From the blue line to the purple, d is 4 to 8. For this figure we took $\mu = 0$.

Because the AdS effect here causes only the constant shift to the flat potential, the photon sphere always exists. Denoting the location of the photon sphere as $r = r_{\text{PS}}$, we find the location in the large l limit

$$r_{\text{PS}} \simeq \left(\frac{d-1}{2} \right)^{1/(d-3)} r_0 =: \tilde{r}. \quad (2.7)$$

Therefore, the photon sphere must exist for any values of the parameters d and r_0 , taking a sufficiently large but finite l .

Indeed, we can numerically confirm that there is a minimum angular momentum l_{\min} such that the photon sphere exists for any $l > l_{\min}$ (Fig. 2). The value of l_{\min} increases as the Hawking temperature T does. Now we note that T grows monotonically with respect to r_0 when T is above the Hawking-Page transition temperature $T_c = (d-2)/2\pi l_0$, that is, $r_0 > 2^{1/(d-3)} l_0$.

We can estimate the expression of $l_{\min} = l_{\min}(r_0)$ with an analytic calculation. In [12], the critical value l_{\min} of the angular momentum has been found as a solution of $V'(r_{\text{PS}}) = V''(r_{\text{PS}}) = 0$ and obtained in a large μ limit. Now, instead, we provide the expression for $\mu = 0$, at a large l . It is expected that the location of the photon sphere r_{PS} approaches the geodesic one (2.7) as l increases. The difference can be estimated in the large l expansion, as

$$r_{\text{PS}} = \tilde{r} - \frac{V'(\tilde{r})}{V''(\tilde{r})} + \mathcal{O}\left(\frac{1}{l^3}\right). \quad (2.8)$$

Regarding the condition that the photon sphere exists, which is expressed as $V''(r_{\text{PS}}) < 0$, as the restriction for l , the value of l is bounded from below by a bound given by the function of r_0 . If we naively use the expression of V'' and (2.8) and truncate them at the first subleading order in the large l expansion, we find the following expression for the lower

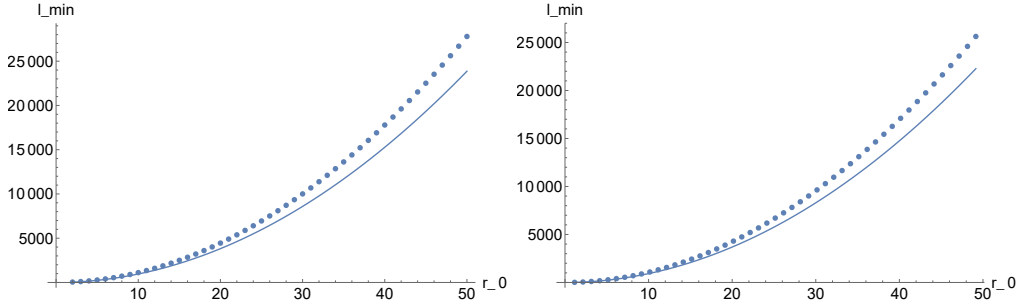


Figure 3. The r_0 -dependence of l_{\min} in $d = 4$ (left panel) and $d = 8$ (right panel). The dotted lines and the solid lines represent the numerical calculation and the analytic estimation (2.9) respectively.

bounds, for example:

$$\begin{aligned}
 d = 4 : \quad l^2 &> \frac{729}{8} \left(\frac{r_0}{l_0}\right)^4 + \frac{9}{2} \left(\frac{r_0}{l_0}\right)^2 - \frac{4}{3}, \\
 d = 8 : \quad l^2 &> \frac{78}{5} 2^{\frac{1}{5}} 7^{\frac{4}{5}} \left(\frac{r_0}{l_0}\right)^4 + 9 \left(\frac{2}{7}\right)^{\frac{3}{5}} \left(\frac{r_0}{l_0}\right)^2 - \frac{690}{49}.
 \end{aligned} \tag{2.9}$$

Fig. 3 is the plot of these analytic bounds (solid lines) and the actual lower bound found numerically (dots). The qualitative behavior of l_{\min} is well captured.² From the analytic estimate, we find that the minimum angular momentum l_{\min} would grow as $\mathcal{O}(r_0^2)$, that is, as $\mathcal{O}(T^{2(d-1)/(d-3)})$.

3 From quasinormal modes to quantum mechanics

In this section we derive a quantum mechanical model which provides the quasinormal mode spectra, in the large angular momentum approximation. The goal is, from the equation (2.2), in the large l approximation, to derive a potential problem of the form

$$\left(-\frac{d^2}{dx^2} + \tilde{V}(x) \right) \psi(x) = E\psi(x), \tag{3.1}$$

where the potential $\tilde{V}(x)$ is approximated by $\tilde{V}(x) \simeq -\frac{x^2}{4}$ around the top of the potential $x = 0$.

3.1 Potential hill relates to the quantum-mechanical model

When the photon sphere exists, we can always expand the potential around the photon sphere. First, let us evaluate the potential $V(r)$ given in (2.4) around the top of the potential,

$$V(r) = V(r_{\text{PS}}) + \frac{1}{2}(r - r_{\text{PS}})^2 V''(r_{\text{PS}}) + \dots \tag{3.2}$$

²The difference between the analytic estimation and the numerical one grows as r_0 (or T) increases. In the derivation of the bound (2.9), we adopt a naive truncation at the first sub-leading order, while the leading $\mathcal{O}(l^2)$ term and the sub-leading $\mathcal{O}(l^0)$ term are comparable to each other. It means that the expression (2.9) is not compatible with the large l expansion. We do not locate the reason why nevertheless (2.9) looks a good approximation in Fig. 3.

Note that here V'' is negative. Then converting the coordinate r to the tortoise coordinate r_* near the top, and denote the difference from the top as δr_* in the tortoise coordinate, we obtain

$$V = V(r_{\text{PS}}) + \frac{1}{2}(\delta r_*)^2 V''(r_{\text{PS}}) f(r_{\text{PS}})^2 + \dots \quad (3.3)$$

Then we perform the following coordinate transformation

$$x \equiv (-2V''(r_{\text{PS}})f(r_{\text{PS}})^2)^{1/4} \delta r_*. \quad (3.4)$$

Together with the definition

$$E \equiv \frac{1}{\sqrt{-2V''(r_{\text{PS}})f(r_{\text{PS}})^2}} (\Omega^2 - V(r_{\text{PS}})), \quad (3.5)$$

we arrive at the equation (3.1) with

$$\tilde{V}(x) = -\frac{x^2}{4} + \mathcal{O}(x^3). \quad (3.6)$$

Next, we shall evaluate the potential $\tilde{V}(x)$ and the relation (3.5) in various limits, including the large l expansion and the high temperature limit $r_0 \gg l_0$.

3.2 Large l expansion

3.2.1 Quasinormal modes and quantum mechanical spectrum

We can evaluate the coefficients in (3.5), in the large l approximation. First, we redefine the frequency as

$$\Omega = \sqrt{V(r_{\text{PS}})} + \tilde{\Omega}. \quad (3.7)$$

At large l , this amounts to looking closely at the energy region near the photon sphere, since we regard $\tilde{\Omega}$ to be $\mathcal{O}(l^0)$, that is, parametrically smaller compared to $\sqrt{V(r_{\text{PS}})}$. Using the definition (3.7), the relation (3.5) is rewritten as

$$\Omega = \sqrt{V(r_{\text{PS}})} + f(r_{\text{PS}}) \sqrt{\frac{-V''(r_{\text{PS}})}{2V(r_{\text{PS}})}} E - \frac{1}{2\sqrt{V(r_{\text{PS}})}} \tilde{\Omega}^2. \quad (3.8)$$

In the large l expansion, the first term is $\mathcal{O}(l)$, and the second term is $\mathcal{O}(l^0)$, while the third term is $\mathcal{O}(l^{-1})$. This means that, in the large l expansion, we find

$$\Omega = a + bE + \mathcal{O}(l^{-1}), \quad (3.9)$$

where

$$a \equiv \sqrt{V(r_{\text{PS}})}, \quad b \equiv f(r_{\text{PS}}) \sqrt{\frac{-V''(r_{\text{PS}})}{2V(r_{\text{PS}})}}. \quad (3.10)$$

An explicit large l expansion leads to

$$a = \sqrt{\left(\frac{1}{l_0^2} + \frac{1}{r_0^2} \frac{d-3}{d-1} \left(\frac{2}{d-1}\right)^{2/(d-3)}\right) \left(l + \frac{d}{2} - 1\right) \left(l + \frac{d}{2} - 2\right) + \mathcal{O}(l^{-1})}, \quad (3.11)$$

$$b = \sqrt{(d-3) \left(\frac{1}{l_0^2} + \frac{1}{r_0^2} \frac{d-3}{d-1} \left(\frac{2}{d-1}\right)^{2/(d-3)}\right) + \mathcal{O}(l^{-2})}. \quad (3.12)$$

So, in summary, we find a formula for the relation between the quasinormal mode spectra Ω and the quantum mechanical energy E of (3.1) in the large l approximation as

$$\Omega = \sqrt{\left(\frac{1}{l_0^2} + \frac{1}{r_0^2} \frac{d-3}{d-1} \left(\frac{2}{d-1}\right)^{2/(d-3)}\right) \left[\sqrt{\left(l + \frac{d}{2} - 1\right) \left(l + \frac{d}{2} - 2\right) + \sqrt{d-3} E} + \mathcal{O}(l^{-1})\right]}. \quad (3.13)$$

Once one solves the quantum mechanical model (3.1), substituting E into the equation above derives the quasinormal mode spectra Ω in the large angular momentum approximation.

3.2.2 On the validity of inverted harmonic oscillator

While the energy spectra E to be substituted into (3.13) will be evaluated in the following section, we here study the shape of the potential $V(x)$. It is an inverted harmonic potential around the top of the potential, and we will see how good the approximation is at large l .

Near the photon sphere at $r = r_{\text{PS}}$, the potential is expanded with the displacement $\delta r \ll r_{\text{PS}}$ as

$$V(r_{\text{PS}} + \delta r) = V(r_{\text{PS}}) + \frac{1}{2} V''(r_{\text{PS}}) (\delta r)^2 + \frac{1}{3!} V^{(3)}(r_{\text{PS}}) (\delta r)^3 + \dots. \quad (3.14)$$

This is approximated by an inverted harmonic oscillator when δr satisfies

$$\delta r \ll \frac{3V''(r_{\text{PS}})}{V^{(3)}(r_{\text{PS}})}. \quad (3.15)$$

This means that the approximation by the inverted harmonic oscillator is valid in the range

$$V(r_{\text{PS}}) \geq V(r) \gg V(r_{\text{PS}}) + \frac{9}{2} \frac{(V''(r_{\text{PS}}))^3}{(V^{(3)}(r_{\text{PS}}))^2}. \quad (3.16)$$

The potential range $\Delta V = |9(V''(r_{\text{PS}}))^3/2(V^{(3)}(r_{\text{PS}}))^2|$ is of $\mathcal{O}(l^2)$, and the range is wide enough for a large l . Therefore, as long as the energy Ω^2 of the quasinormal mode is in this range, one expects a safe use of the inverted harmonic potential. However, as we will discuss below, we argue that the spectra are not determined solely by the potential shape near the top.

3.2.3 AdS boundary is a hard wall

Let us turn to the shape of the potential near the AdS boundary. We will show that the AdS boundary can be regarded as a hard-wall potential, where a Dirichlet condition is imposed on the field.

Near the boundary $r \sim \infty$, the tortoise coordinate (2.3) is well-approximated as

$$r_* = -\frac{l_0^2}{r}, \quad (3.17)$$

because the effect of the black hole disappears and the geometry is almost equal to that of the pure AdS. Using this expression, the potential $V(r)$ in (2.4) is approximated as

$$V \simeq \frac{1}{l_0^2} \left(l + \frac{d}{2} - 1 \right) \left(l + \frac{d}{2} - 2 \right) + \frac{1}{r_*^2} \left[\frac{d}{2} \left(\frac{d}{2} - 1 \right) + \mu^2 l_0^2 \right]. \quad (3.18)$$

The second term diverges at the AdS boundary $r_* = 0$. So, it works as a wall by which any wave is bounced back.

The reason why this is a hard wall is as follows. In the large l limit, the first term in (3.18) is pushed up as a constant but being very high. The effect of the second term appears only when these two terms are comparable,

$$r_* \sim l_0 \left[\frac{d}{2} \left(\frac{d}{2} - 1 \right) + \mu^2 l_0^2 \right]^{1/2} \frac{1}{l}, \quad (3.19)$$

at a large l . This point is very close to the AdS boundary $r_* = 0$, and in the large l limit, it coincides with the AdS boundary. Therefore, the AdS boundary behaves as a hard wall at a large l .

The existence of the hard wall is crucial in the analysis, as we will find in the next section. In fact, the difference between the asymptotically flat case and the AdS case was already noted in [20].

3.3 Analytic potential at high temperature

In the above, we saw that the potential is approximated by the inverted harmonic oscillator around the top, and there exists a hard wall at the AdS boundary. In the next section we evaluate E in systems which possess these characteristics. In this subsection, we consider the case of a high temperature and will find an analytic shape of the potential $\tilde{V}(x)$ which actually possesses the features described above.³

First, we evaluate the tortoise coordinate (2.3) as

$$r_* = \int_{\infty}^r dr' \left[1 + \frac{(r')^2}{l_0^2} - \frac{r_0^{d-3}}{(r')^{d-3}} \right]^{-1} = r_0 \int_{\infty}^{r/r_0} ds \left[1 - \frac{1}{s^{d-3}} + \frac{r_0^2}{l_0^2} s^2 \right]^{-1}, \quad (3.20)$$

³Note that we take the limit $l \rightarrow \infty$ first and then a high temperature limit, otherwise the potential hill would disappear as we described in Sec. 2.

where we made a change of variable $s \equiv r/r_0$. It is understood that in the high temperature case $r_0 \gg l_0$, we find an approximation

$$r_* \simeq r_0 \int_{\infty}^{r/r_0} ds \left[\frac{r_0^2}{l_0^2} s^2 \right]^{-1} = -\frac{l_0^2}{r} \quad (3.21)$$

as long as

$$r \gg r_0^{\frac{d-3}{d-1}} l_0^{\frac{2}{d-1}}. \quad (3.22)$$

Note that the latter condition is satisfied for the photon sphere $r = r_{\text{PS}}$ given in (2.7) at large l , under the high temperature condition $r_0 \gg l_0$. Thus, although (3.21) is exactly the same as the near-boundary expression (3.17), we can use it even near the top of the potential, at high temperature.

Using (3.21), the large l potential (2.6) is written as

$$V \simeq l^2 \left[\frac{1}{l_0^2} + \frac{1}{l_0^4} r_*^2 - \frac{r_0^{d-3}}{l_0^{2(d-1)}} (-r_*)^{d-1} \right] \quad \left(r_* < 0, |r_*| \ll r_0^{\frac{3-d}{d-1}} l_0^{\frac{2(d-2)}{d-1}} \right) \quad (3.23)$$

$$V = \infty \quad (r_* \geq 0) \quad (3.24)$$

The latter is to make sure that there exists a hard wall at $r_* = 0$, as explained in the previous subsection. The potential is the same as the one found in [12] at a WKB approximation.

With the linear redefinition (3.4) of r_* , we can rewrite this potential into the form (3.1). A simple calculation leads to the quantum mechanical potential $\tilde{V}(x)$ whose hill top is located at $x = 0$ with the hard wall located at $x = L$,

$$\tilde{V}(x) = \frac{1}{4(d-3)} \left[(L-x)^2 - \beta^{d-3} (L-x)^{d-1} - \left(L^2 - \beta^{d-3} L^{d-1} \right) \right], \quad (3.25)$$

where

$$\beta \equiv (d-3)^{-1/4} 2^{-1/2} \frac{1}{\sqrt{l}} \frac{r_0}{l_0}, \quad L \equiv \beta^{-1} \left(\frac{2}{d-1} \right)^{\frac{1}{d-3}}. \quad (3.26)$$

Note that in these expressions we keep only leading terms at the high temperature $r_0 \gg l_0$ and also the large l , and we have adjusted the constant term of the potential so that the height of the potential top is tuned to $\tilde{V} = 0$, for our later purpose.

To illustrate this potential, we consider the case $d = 4$. We obtain

$$\tilde{V}(x) = -\frac{1}{4} x^2 + 2^{-5/2} \frac{1}{\sqrt{l}} \frac{r_0}{l_0} x^3, \quad (3.27)$$

and the wall position is at

$$L = \frac{2^{3/2}}{3} \sqrt{l} \frac{l_0}{r_0}. \quad (3.28)$$

The system is defined in the region $x < L$, and all waves are reflected at the AdS boundary hard wall $x = L$. The potential approximation is not trusted for large negative values

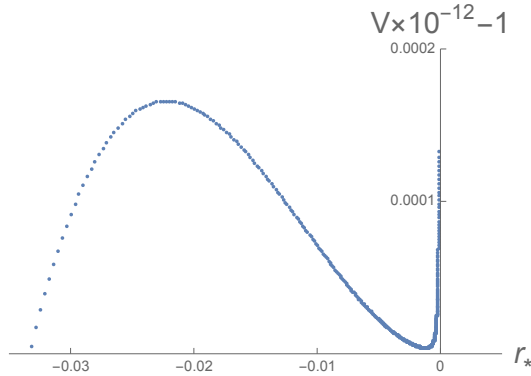


Figure 4. The effective potential V in the tortoise coordinate r_* , at high temperature. For this figure we took $d = 4$, $\mu = 0$, $r_0 = 30$, $l = 10^6$, in the unit $l_0 = 1$.

of x . In Fig. 4, we plot the potential (2.4) numerically evaluated at high temperature $r_0/l_0 = 30 \gg 1$. We can confirm the potential shape (3.25), with the hard wall at the AdS boundary.

How far is this wall from the top of the hill? The existence condition of the photon sphere (2.9) shows, at high temperature $r_0/l_0 \gg 1$, that we have the condition $l^2 \gg \mathcal{O}((r_0/l_0)^4)$. The wall location (3.28) then implies $L \gg \mathcal{O}(1)$. We conclude that the wall is located very far from the potential hill, in the metric of this x space. In addition, note that near the wall the potential approaches a new bottom, $V'(L) = 0$, which means that the whole potential cannot exactly be equal to the inverted harmonic potential for any choice of the wall position.

4 Solving quasinormal modes respecting AdS boundary

In this section, we analyze the quasinormal mode spectrum by solving quantum mechanical models, through the relation studied in Sec. 3. The potential of the quantum mechanical model (3.1) is obtained only in numerical manner, and it is numerically demanding to calculate the spectrum at the large l , as mentioned in [10]. Thus instead, we use solvable models, the inverted harmonic oscillator and the Pöschl-Teller model, which share the same shape of the potential as that of (3.1). We show that the discrete spectrum is located on a peculiar curve in the complex energy E -plane, reflecting the potential hill of a photon sphere and the AdS boundary. The effect of the boundary does not vanish even when the boundary is sent to the spatial infinity since decaying modes $\text{Im } E < 0$ grow near the boundary. The solvable models result in the unique pattern of the spectrum, and in particular, the curve is rather insensitive to the shape of the potential tail. This universality leads us to state that the pattern of the QNM spectrum is captured by that of the solvable models.

4.1 Inverted harmonic oscillator

Recall that the Kellin-Gordon equation on the AdS Schwarzschild background reduces to a quantum mechanical model (3.1). The potential has a hill $\tilde{V}(x) \simeq -\frac{x^2}{4}$ whose top

corresponds to the photon sphere. The energy E is measured from the top of the hill.

In this subsection we replace the potential with the exact inverted harmonic potential

$$\tilde{V}(x) \rightarrow -\frac{x^2}{4}, \quad (4.1)$$

and solve the Schrödinger equation

$$\left(-\frac{d^2}{dx^2} - \frac{x^2}{4}\right)\psi(x) = E\psi(x). \quad (4.2)$$

We impose the Dirichlet boundary condition,

$$\psi(L) = 0, \quad L \gg 1. \quad (4.3)$$

Also we assume that the wave function $\psi(x)$ has only the out-going mode in a region $x \rightarrow -\infty$ so that the amplitude decays with respect to time. The potential hill at $x = 0$ represents the photon sphere, while the Dirichlet boundary at $x = L$ represents the AdS boundary. The out-going mode in the region $x \rightarrow -\infty$ corresponds to a scalar mode that is absorbed by the black hole: the horizon condition.

The Schrödinger equation is solvable⁴, and its solution is called the parabolic cylinder function. Changing the two variables x, E into z, ν as

$$z \equiv e^{+i\pi/4}x, \quad E \equiv +i\left(\nu + \frac{1}{2}\right), \quad (4.4)$$

the general form of the solution is written as

$$\psi = A \cdot D_\nu(z) + B \cdot D_{-\nu-1}(iz), \quad (4.5)$$

where A, B are some constants.

The parabolic cylinder function $D_\nu(z)$ has an asymptotic form

$$D_\nu(z) \sim \begin{cases} e^{-z^2/4}z^\nu - \frac{\sqrt{2\pi}}{\Gamma(-\nu)}e^{\pm i\pi\nu}e^{z^2/4}z^{-\nu-1} & \pi/4 < \pm \arg z < 5\pi/4 \\ e^{-z^2/4}z^\nu & -3\pi/4 < \arg z < 3\pi/4 \end{cases} \quad (4.6)$$

For our later convenience, we introduce a function

$$\vartheta_\pm(\nu; z) \equiv \frac{-iz^2}{2} + i(2\nu + 1) \ln z \pm \pi\nu - i \ln \frac{\sqrt{2\pi}}{\Gamma(-\nu)} \quad (4.7)$$

so that the location of zeros of the wave function is easily spotted,

$$D_\nu(z) \sim e^{-z^2/4}z^\nu (1 - e^{i\vartheta_\pm(\nu; z)}), \quad \pi/4 < \pm \arg z < 5\pi/4. \quad (4.8)$$

By using the form of the asymptotic expansion, we find that the parabolic cylinder function $D_\nu(z)$ has an in-going mode in the region $x \rightarrow +\infty$ and has in/out-going modes in the region $x \rightarrow -\infty$, whereas $D_{-\nu-1}(iz)$ has in/out-going modes in the region $x \rightarrow +\infty$ and

⁴See App. B.1 for more detailed discussion on the spectrum.

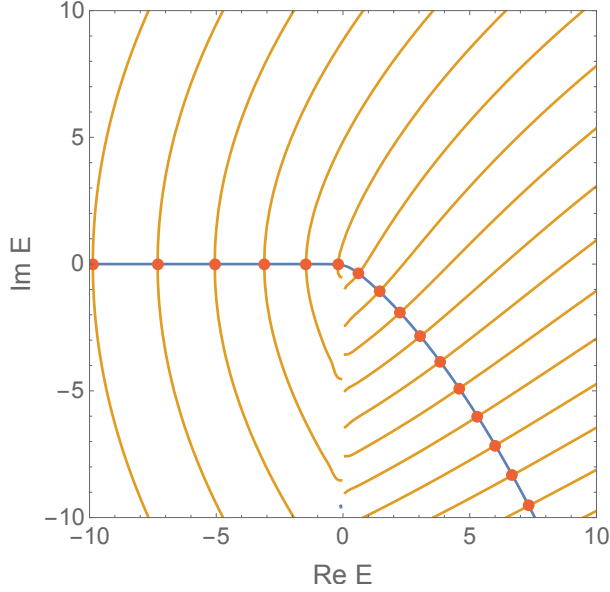


Figure 5. The spectrum of the inverted harmonic oscillator $\tilde{V}(x) = -\frac{x^2}{4}$ (indicated as red blobs). We have imposed the Dirichlet boundary condition at $x = L = 10$, and have assumed that there is only the out-going mode in the region $x \rightarrow -\infty$. The blue curve represents $\text{Im } \vartheta_+ = 0$, while the orange curve represents $\text{Re } \vartheta_+ \in 2\pi\mathbf{Z}$. The intersection points of the two curves represent the quantized energy spectrum.

has an out-going mode in the region $x \rightarrow -\infty$. Thus the appropriate choice of the solution is

$$\psi = B \cdot D_{-\nu-1}(iz). \quad (4.9)$$

Near the boundary $x \sim L \gg 1$, the wave function takes the following form,

$$\psi \sim e^{-(iz)^2/4} (iz)^{-\nu-1} \left(1 - e^{i\vartheta_+(-\nu-1; iz)} \right). \quad (4.10)$$

Thus the Dirichlet boundary condition $0 = \psi(L)$ yields a quantization condition,

$$\vartheta_+(-\nu-1; iz) \in 2\pi\mathbf{Z}. \quad (4.11)$$

That is, more explicitly,

$$\frac{\pi}{2} + \frac{L^2}{2} + \left(2 \ln L + \frac{\pi i}{2} \right) E + i \ln \frac{\sqrt{2\pi}}{\Gamma(1/2 - iE)} \in 2\pi\mathbf{Z}. \quad (4.12)$$

The spectrum in the complex E -plane is plotted in Fig. 5. The blue/orange curves are for $\text{Im } \vartheta_+ = 0, \text{Re } \vartheta_+ \in 2\pi\mathbf{Z}$, respectively. The intersection points of the two curves are the solutions of the quantization condition.

The solutions in the region $\text{Re } E < 0$ have almost vanishing imaginary part, and correspond to extremely stable quasinormal modes localized in the region between the photon sphere potential and the AdS boundary. The existence of these modes were already pointed out by [12], and our result is consistent with that.

The spectrum in the region $\text{Re } E > 0$ and $\text{Im } E < 0$ corresponds to unstable quasinormal modes above the top of the potential hill of the photon sphere. The whole spectrum is located on the following peculiar curve in the complex E -plane,

$$0 = \text{Im} \left[\left(2 \ln L + \frac{\pi i}{2} \right) E + i \ln \frac{\sqrt{2\pi}}{\Gamma(1/2 - iE)} \right]. \quad (4.13)$$

This is a curve whose negative imaginary part of E grows when the real part of E grows, see Fig. 5.

Let us consider the large angular momentum limit $l \rightarrow \infty$. As seen in (3.26), it corresponds to the large L limit in the original quantum mechanical model. When the boundary is sent to the spatial infinity, $L \rightarrow +\infty$, the slope of the curve (4.13) in the E -plane decreases and the curve approaches the positive real axis. In fact, expanding the gamma function $\Gamma(1/2 - iE)$ around $E = 0$, we find

$$E \sim \frac{\pi}{\ln L} \left\{ n - \left(\frac{L^2}{4\pi} - \left\lfloor \frac{L^2}{4\pi} \right\rfloor \right) - \frac{1}{4} - \frac{i \ln 2}{4\pi} \right\}, \quad n = 1, 2, \dots \ll \ln L. \quad (4.14)$$

The quantum number n counts the QNM, and the imaginary part of the spectrum E becomes a constant negative value independent of n .

Before closing this subsection, it will be worthwhile to compare this spectrum to the one with different boundary conditions. Suppose that we instead allow only out-going modes on both sides of the potential hill, $x \rightarrow \pm\infty$. The spectrum is obtained by killing the in-going mode of $\psi = B \cdot D_{-\nu-1}(iz)$ in the region $x \rightarrow +\infty$ by setting

$$-\frac{\sqrt{2\pi}}{\Gamma(1+\nu)} e^{+i\pi(-1-\nu)} = 0. \quad (4.15)$$

The gamma function has poles at non-positive integers, thus,

$$E = -i \left(n + \frac{1}{2} \right), \quad n = 0, 1, 2, \dots \quad (4.16)$$

The apparent mismatch between (4.16) and (4.14) in the limit $L \rightarrow \infty$ is not a contradiction. In our case of (4.14), for a decaying solution $\text{Im } E < 0$, the out-going mode of $D_{-\nu-1}(iz)$ grows in power as x approaches the boundary, whereas the in-going mode decreases in power. Thus we needed to add an in-going mode with a large amplitude coefficient to realize the Dirichlet boundary condition. This is different from just having the out-going mode. Therefore, the existence of the hard wall, even placed at the spatial infinity, discontinuously changes the spectrum.

4.2 Pöschl-Teller model

In this subsection, we demonstrate that the curve (4.13) is almost insensitive to the shape of the potential tail in a solvable model. We replace the potential of the quantum mechanical model (3.1) with that of the Pöschl-Teller type,

$$\tilde{V}(x) \rightarrow V_0 \left(\frac{1}{\cosh^2 \alpha x} - 1 \right). \quad (4.17)$$

The top of the hill in this potential is approximated by the inverted harmonic potential, while the potential has a potential tail which resembles the actual shape of the potential near the AdS boundary, (3.25). For our later convenience, we introduce a variable

$$\omega^2 = V_0 + E, \quad (4.18)$$

and consider the Schrödinger equation with the Pöschl-Teller potential⁵

$$\left[\frac{d^2}{dx^2} + \omega^2 - \frac{V_0}{\cosh^2 \alpha x} \right] \psi(x) = 0, \quad (4.19)$$

where

$$V_0 \equiv \alpha^2 \lambda(1 - \lambda), \quad (4.20)$$

$$\alpha > 0, \quad \lambda \equiv \frac{1}{2} + i\nu, \quad \nu > 0. \quad (4.21)$$

In a manner similar to the inverted harmonic oscillator, we shall solve this Schrödinger equation under the Dirichlet boundary condition,

$$\psi(L) = 0, \quad L \gg 1. \quad (4.22)$$

Also we assume that the wave function $\psi(x)$ has only the out-going mode in the region $x \rightarrow -\infty$, under the condition that the wave function decays with respect to time, $\text{Im } E = \text{Im } \omega^2 < 0$.

The Schrödinger equation has two independent solutions (see Eq.(9) in [38]):

$$f_+(x) = e^{i\omega x} F\left(\lambda, 1 - \lambda; \frac{e^{\alpha x}}{e^{\alpha x} + e^{-\alpha x}}\right), \quad (4.23)$$

$$f_-(x) = (e^{\alpha x} + e^{-\alpha x})^{\frac{i\omega}{\alpha}} F\left(\lambda - \frac{i\omega}{\alpha}, 1 - \lambda - \frac{i\omega}{\alpha}; \frac{e^{\alpha x}}{e^{\alpha x} + e^{-\alpha x}}\right). \quad (4.24)$$

Here F is the hypergeometric function. Transforming variables, we find

$$\begin{aligned} f_+(x) &= e^{i\omega x} \frac{\Gamma(1 + i\omega/\alpha)\Gamma(i\omega/\alpha)}{\Gamma(\lambda + i\omega/\alpha)\Gamma(1 - \lambda + i\omega/\alpha)} F\left(\lambda, 1 - \lambda; \frac{1}{e^{2\alpha x} + 1}\right) \\ &\quad + (e^{\alpha x} + e^{-\alpha x})^{-i\omega/\alpha} \frac{\Gamma(1 + i\omega/\alpha)\Gamma(-i\omega/\alpha)}{\Gamma(\lambda)\Gamma(1 - \lambda)} F\left(\lambda + i\omega/\alpha, 1 - \lambda + i\omega/\alpha; \frac{1}{e^{2\alpha x} + 1}\right) \\ &\sim \begin{cases} e^{i\omega x} & (\text{Im } \omega > 0, x \rightarrow -\infty) \\ e^{i\omega x} \frac{\Gamma(1 + i\omega/\alpha)\Gamma(i\omega/\alpha)}{\Gamma(\lambda + i\omega/\alpha)\Gamma(1 - \lambda + i\omega/\alpha)} \\ \quad + e^{-i\omega x} \frac{\Gamma(1 + i\omega/\alpha)\Gamma(-i\omega/\alpha)}{\Gamma(\lambda)\Gamma(1 - \lambda)} & (\text{Im } \omega > 0, x \rightarrow +\infty) \end{cases} \quad (4.25) \\ f_-(x) &= (e^{\alpha x} + e^{-\alpha x})^{i\omega/\alpha} \frac{\Gamma(1 - i\omega/\alpha)\Gamma(i\omega/\alpha)}{\Gamma(\lambda)\Gamma(1 - \lambda)} F\left(\lambda - i\omega/\alpha, 1 - \lambda - i\omega/\alpha; \frac{1}{e^{2\alpha x} + 1}\right) \end{aligned}$$

⁵See App. B.2 for more detailed discussion on the spectrum.

$$\begin{aligned}
& + e^{-i\omega x} \frac{\Gamma(1-i\omega/\alpha)\Gamma(-i\omega/\alpha)}{\Gamma(\lambda-i\omega/\alpha)\Gamma(1-\lambda-i\omega/\alpha)} F\left(\lambda, 1-\lambda; \frac{1}{1+i\omega/\alpha}; \frac{1}{e^{2\alpha x}+1}\right) \\
\sim & \begin{cases} e^{-i\omega x} & (\text{Im } \omega < 0, x \rightarrow -\infty) \\ e^{i\omega x} \frac{\Gamma(1-i\omega/\alpha)\Gamma(i\omega/\alpha)}{\Gamma(\lambda)\Gamma(1-\lambda)} & \\ + e^{-i\omega x} \frac{\Gamma(1-i\omega/\alpha)\Gamma(-i\omega/\alpha)}{\Gamma(\lambda-i\omega/\alpha)\Gamma(1-\lambda-i\omega/\alpha)} & (\text{Im } \omega < 0, x \rightarrow +\infty) \end{cases} \quad (4.26)
\end{aligned}$$

Thus the appropriate choice of the solution is

$$\psi \propto f_-(x). \quad (4.27)$$

Near the boundary $x \sim L \gg 1$, the wave function takes the following form

$$\psi \sim e^{i\omega x} \frac{\Gamma(1-i\omega/\alpha)\Gamma(i\omega/\alpha)}{\Gamma(\lambda)\Gamma(1-\lambda)} \left(1 - e^{i\vartheta(\omega;x)}\right), \quad (4.28)$$

where

$$\vartheta(\omega;x) \equiv \pi - 2\omega x - i \ln \frac{\Gamma(-i\omega/\alpha)}{\Gamma(i\omega/\alpha)} \frac{\Gamma(\lambda)\Gamma(1-\lambda)}{\Gamma(\lambda-i\omega/\alpha)\Gamma(1-\lambda-i\omega/\alpha)}. \quad (4.29)$$

The Dirichlet boundary condition $0 = \psi(L)$ yields the following quantization condition,

$$\vartheta(\omega, L) \in 2\pi\mathbf{Z}. \quad (4.30)$$

Its spectrum is plotted in the left panel of Fig. 6. The blue/orange curves are for $\text{Im } \vartheta = 0$, $\text{Re } \vartheta \in 2\pi\mathbf{Z}$, respectively. Their intersection points are the solutions of the quantization condition. The parameters in the potential are chosen so that $\tilde{V}(x) \simeq -\frac{x^2}{4}$ around the top of the potential hill, to be compared with the result of the inverted harmonic oscillator, Fig. 5.

As in the case of the inverted harmonic oscillator, the spectrum in the region $\text{Re } E < 0$ has almost vanishing imaginary part, and corresponds to extremely stable quasinormal modes living in the spatial region between the photon sphere potential and the AdS boundary. Other spectrum in the region $\text{Re } E > 0$ and $\text{Im } E < 0$ corresponds to unstable modes above the top of the potential hill of the photon sphere. Therefore, we conclude that the spectral pattern of this model shares the same characteristic with that of the inverted harmonic potential.

In the right panel of Fig. 6, we plot the spectrum in the ω -plane, for the readers' reference. In the ω -plane, spectra appear on both sides of positive/negative real axis since there are two branches $\omega = \pm\sqrt{E+V_0}$. One of the blue horizontal curves in the ω -plane is mapped to the blue curve on E -plane.⁶

⁶As a remark aside, one observes other series of complex solutions in the ω -plane: the intersection points of two blue vertical curves and series of orange curves around the origin, see the central part of the right panel of Fig. 6. Such a series of solutions is mapped to the region $\text{Re } E < -V_0 = -10$, which is below the bottom of the potential defined by the potential tail. Thus it is natural to regard it as an unphysical series of solutions and we ignored it. It would be interesting if this unphysical series of solutions allow some holographic interpretation, in quantum path-integral.

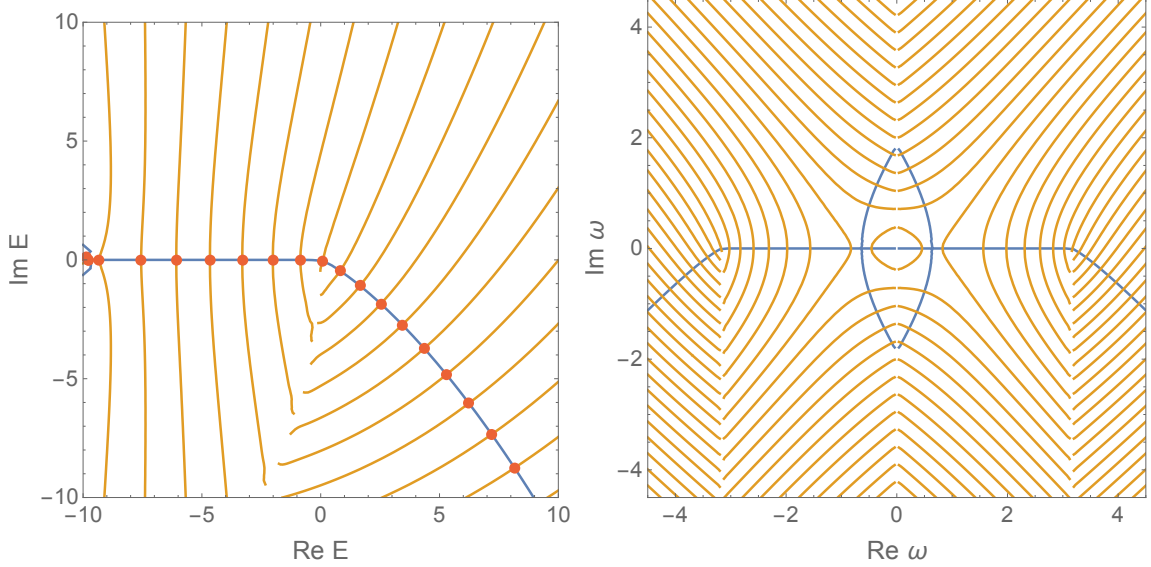


Figure 6. The spectrum of the Pöschl-Teller type potential $\tilde{V}(x) = V_0 \left(\frac{1}{\cosh^2 \alpha x} - 1 \right)$ with $V_0 = 10$ (indicated as red blobs). We have imposed the Dirichlet boundary condition at $x = L = 10$, and have assumed that there is only the out-going mode in the region $x \rightarrow -\infty$. Other parameters are tuned as $\alpha = 1/\sqrt{4V_0}$, $\nu = \sqrt{4V_0^2 - 1}/4$ so that we keep $\tilde{V}(x) \simeq -\frac{x^2}{4}$ around the top of the potential hill, to be compared with Fig. 5. The blue curve represents $\text{Im } \vartheta = 0$, while the orange curve represents $\text{Re } \vartheta \in 2\pi\mathbf{Z}$. Their intersection points represent the quantized energy spectrum. The left (right) panel is the spectrum in the E -plane (ω -plane).

We can show that the equation for the blue curve $\text{Im } \vartheta = 0$ approaches that of the inverted harmonic oscillator when the height of the potential V_0 is sent to the infinity. Let us fix the parameters as

$$\alpha = \frac{1}{\sqrt{4V_0}}, \quad \nu = \sqrt{4V_0^2 - \frac{1}{4}} \quad (4.31)$$

so that $\tilde{V}(x) \simeq -\frac{x^2}{4}$ near the top of the potential hill, then send the potential height to a large value. Some straightforward calculations of (4.29) with the Stirling's formula show that

$$\vartheta(\omega; x) \sim (\text{Real const.}) - \left(2 \ln L_{\text{eff.}} + \frac{\pi i}{2} \right) E - i \ln \frac{\sqrt{2\pi}}{\Gamma(1/2 - iE)}, \quad (4.32)$$

where $2 \ln L_{\text{eff.}} \equiv \frac{L}{\sqrt{V_0}} + \ln V_0$. Thus the curve on which quasinormal modes are located is

$$0 = \text{Im} \left[\left(2 \ln L_{\text{eff.}} + \frac{\pi i}{2} \right) E + i \ln \frac{\sqrt{2\pi}}{\Gamma(1/2 - iE)} \right], \quad (4.33)$$

which is exactly the same form as (4.13).

Our results in the inverted harmonic oscillator and in the Pöschl-Teller type potential imply that quasinormal modes near the photon sphere appear with a peculiar spectral pattern, in the large angular momentum sector. The pattern is shown in Fig. 5 and Fig. 6, and it is on a curve of the form given by (4.13).

5 Summary and discussion

In this paper, we calculated the spectrum Ω of the scalar quasinormal mode (QNM) associated with the photon sphere in the AdS Schwarzschild black hole. In the large l limit where l is the angular momentum of the QNM, we found that Ω is related to the energy spectrum E of the quantum mechanics (QM) (3.1), as given in (3.13). At high temperature, the QM potential was analytically calculated as (3.25). The QM is not solvable analytically, so we instead analytically solved the inverted harmonic oscillator with a hard wall as (4.12), to obtain the feature of the QM spectrum E . The resultant E is a discrete series along a curve on the complex E -plane. As we see in Fig. 5, $\text{Im } E$ (which needs to be negative as it is for decaying modes) grows in its magnitude as $\text{Re } E$ grows, while $\text{Im } E$ almost vanishes for negative $\text{Re } E$. Quite a similar pattern of the spectrum is universally obtained in the Pöschl-Teller model with a hard wall (see Fig. 6), which suggests that the QM has the same spectral feature, which is translated to the feature of the QNMs through the relation (3.13). This spectrum, by the AdS/CFT dictionary, should be equal to the spectrum of a thermal holographic CFT on a sphere whose radius is l_0 , at the large angular momentum l .

An interesting feature of the obtained QNM spectrum, (3.13) with (4.12) or (4.30), is the fact that the spectrum whose real part is larger than the photon sphere energy always accompanies a non-vanishing imaginary part which is not directly related to the temperature. Normally the imaginary part of QNMs is due to the boundary condition at the black hole horizon, thus is a direct consequence of the temperature. In the present case, the imaginary part is dictated by the photon sphere, which is determined mainly by the angular momentum. The precise spectrum (3.13) is a prediction to the thermal holographic CFT, and in general holographic QFTs we expect that such a “photon-sphere subsector” exists in their spectrum.

Here note also that the spectrum whose real part is smaller than the photon sphere energy ($\text{Re } E < 0$) has almost vanishing imaginary part, meaning that they are extremely stable. These modes are confined in the radial region bounded by the photon sphere and the AdS boundary. The existence of these modes were already pointed out in [12], and our result is consistent with it.

Let us discuss a dual CFT interpretation of the QNMs which we analyzed in this paper. They should correspond to an operator of the form $\text{tr}[FDDD \cdots DDF]$ where $D = D_\theta$ is the covariant derivative along the equator of the sphere. This type of operator carries a large angular momentum on the sphere. In our analysis, the spectrum consists of (i) those at $\text{Re } E > 0$ with nonzero and growing imaginary part, and (ii) those at $\text{Re } E < 0$ with almost vanishing imaginary part.

The latter (ii) corresponds to the stable states [12], which are localized near the AdS boundary and spinning along the boundary sphere. We see that their energy Ω is given as l/l_0 where l is the angular momentum (and thus the number of D_θ 's in the operator) and l_0 is the radius of the sphere. This is reminiscent of the pp-wave limit and the BMN operators [39], which are stable and dictated by a long spin chain. The stability of these states suggests a bound between the angular momentum and the energy, which reminds

us of the Kerr bound for black hole masses. The bound could be explained by some symmetry; in fact, as is seen in the effective potential (3.23), the system is approximated by a harmonic oscillator around the AdS boundary $r_* = 0$, with the Dirichlet boundary condition at $r_* = 0$. This means that the spectrum of the QNMs localized near the AdS boundary is dictated by an $SL(2; \mathbf{R})$ symmetry (which should also act on the operator space in the CFT). Further study on these states would be interesting.

On the other hand, what we studied in detail in this paper is the sector (i) whose real part of the energy Ω is around the photon sphere, $\text{Re} \Omega \sim l\sqrt{1/l_0^2 + 1/r_0^2}$. This value of the energy is at the top of the potential hill. The QNM develops the imaginary part. The corresponding operator in the CFT side is of the same form, $\text{tr}[FDDD \cdots DDF]$, but with very many impurity operators inserted. When the number of the impurities exceeds the photon sphere bound $\sim l \cdot l_0^2/r_0^2$ (which amounts to the energy difference between the top of the potential hill and the bottom at the AdS boundary), the states becomes suddenly unstable and decays. In other words, the state with the large angular momentum of the form $\text{tr}[FDDD \cdots DDF]$ could be quite stable against large addition of impurities whose number can go up to $\sim l \cdot l_0^2/r_0^2$. This universal behavior of the CFT states, expected through the AdS/CFT duality, may need more intuitive explanation in the CFT language.

In the following, we present several discussions on how our work may be related to some other aspects in AdS/CFT and holography.

- First, let us discuss the relation between our spectra and those found in the asymptotically flat case [4]. As we have emphasized in Sec. 4, our AdS case has a hard wall at the AdS boundary, while the asymptotically flat case does not have the wall. This difference was crucial in determining the spectrum. Now, suppose that we add a flat spacetime joined to the AdS boundary, as was done in [40]. Then the wall could “disappear” and the QNM in the AdS bulk can escape to the joined flat spacetime. Since the AdS plus the joined flat space may allow a holographic interpretation as a CFT joined with a higher dimensional CFT, the spectrum found in [4], which is dictated by the $SL(2; \mathbf{R})$ symmetry, may be realized in the AdS/CFT setup in this manner. It would be interesting to find the AdS/CFT interpretation of the $SL(2; \mathbf{R})$ subsector observed in [4], in view of the issues concerning evaporation of black holes and the Page curve.
- Einstein rings can be obtained in holographic CFT [34, 35] by using an imaging transform on a CFT one-point function.⁷ The CFT is with a point-like source, thus the holographic imaging of the Einstein rings is a direct consequence of two-point functions on the holographic CFT. Since generally the QNM spectrum near the photon sphere should characterize Einstein rings, it would be interesting to find a relation between the image of the holographic Einstein rings and the photon-sphere subsector of the CFT spectrum.

⁷The imaging in holography and string theory has been further developed for various purposes, see Refs. [41–49].

- In the context of the AdS/CFT, Lyapunov exponents have been studied in connection to the chaos bound saturation [50], as it is related to the black hole surface gravity [51–53]. The QNMs associated with the photon sphere naturally defines the Lyapunov exponent there [20], thus its relevance to the chaos bound would be interesting if exists. Namely, the chaos bound could work as a bound for the QNM spectra. This research direction would contribute to some general discussion on the black hole instability, such as [54].

Further interplay between boundary CFTs and photon spheres will reveal the mystery of the AdS/CFT correspondence.

Acknowledgment

We would like to thank K. Yoshida for valuable discussions. The work of K. H. was supported in part by JSPS KAKENHI Grant No. JP22H01217, JP22H05111 and JP22H05115. The work of K. S. was supported in part by Grant-in-Aid for JSPS Fellows No. 23KJ1310. The work of T. Y. was supported in part by JSPS KAKENHI Grant No. JP22H05115 and JP22KJ1896.

A Representation of $SL(2; \mathbf{R})$

We review several properties of $SL(2; \mathbf{R})$ and discuss the representation of its Lie algebra.

A.1 Relation between $SO(2, 1)$, $SU(1, 1)$ and $SL(2; \mathbf{R})$

There are three kinds of noncompact Lie algebras $so(2, 1) \cong su(1, 1) \cong sl(2, \mathbf{R})$ that are isomorphic one another as described in the Fig. 7. They play important roles in physics.

The noncompact group $SL(2; \mathbf{R})$ is the linear group consisting of matrices $g = \begin{pmatrix} \alpha & \beta \\ \gamma & \delta \end{pmatrix}$ ($\alpha, \beta, \gamma, \delta \in \mathbf{R}$) with a relation $\alpha\delta - \beta\gamma = 1$. The $SU(1, 1)$ is the complex linear group generated by $g' = \begin{pmatrix} a & b \\ \bar{b} & \bar{a} \end{pmatrix}$ ($a, b \in \mathbf{C}$) with a constraint $|a|^2 - |b|^2 = 1$.

This $SU(1, 1)$ is isomorphic to $SL(2; \mathbf{R})$ under a similarity transformation $g = t^{-1} \cdot g' \cdot t$ for $g \in SU(1, 1)$ and $g' \in SL(2; \mathbf{R})$ with $t \equiv \frac{1}{\sqrt{2}} \begin{pmatrix} 1 & i \\ i & 1 \end{pmatrix}$. That leads to relations of entries of matrices as $a = \frac{\alpha+\delta}{2} + i\frac{\beta-\gamma}{2}$, $b = \frac{\beta+\gamma}{2} + i\frac{\alpha-\delta}{2}$. As concrete examples, we can consider 1-parameter subgroups of $SL(2; \mathbf{R})$ and their correspondents as $SU(1, 1)$ elements:

$$\text{elliptic}; \begin{pmatrix} \cos \frac{t}{2} & -\sin \frac{t}{2} \\ \sin \frac{t}{2} & \cos \frac{t}{2} \end{pmatrix} \leftrightarrow \begin{pmatrix} e^{-i\frac{t}{2}} & 0 \\ 0 & e^{+i\frac{t}{2}} \end{pmatrix}, \quad (\text{A.1})$$

$$\text{hyperbolic}; \begin{pmatrix} e^{-t/2} & 0 \\ 0 & e^{t/2} \end{pmatrix} \leftrightarrow \begin{pmatrix} \cosh \frac{t}{2} & -i \sinh \frac{t}{2} \\ i \sinh \frac{t}{2} & \cosh \frac{t}{2} \end{pmatrix}, \quad (\text{A.2})$$

$$\text{parabolic}; \begin{pmatrix} 1 & 0 \\ t & 1 \end{pmatrix} \leftrightarrow \begin{pmatrix} 1 - i\frac{t}{2} & \frac{t}{2} \\ \frac{t}{2} & 1 + i\frac{t}{2} \end{pmatrix}. \quad (\text{A.3})$$

$$\begin{array}{ccc}
SO(3,1) & \leftrightarrow & SL(2; \mathbf{C}) \\
\downarrow & & \downarrow \\
SO(2,1) & \leftrightarrow & SU(1,1) \leftrightarrow SL(2; \mathbf{R})
\end{array} \tag{A.4}$$

Figure 7. Non compact groups are related one another. $SO(2,1)$ is constructed by a reduction from $SO(3,1)$. $SU(1,1)$ is obtained from $SL(2; \mathbf{C})$ by a suitable restriction. $SU(1,1)$ is also related to $SL(2; \mathbf{R})$ by a similarity transformation.

The $SU(1,1)$ is a covering space of $SO(2,1)$, and the latter leaves the bilinear form $x_0^2 - x_1^2 - x_2^2$ invariant and is a subgroup of a Lorentz group $SO(3,1)$. The center of $SU(1,1)$ is \mathbf{Z}_2 , and $SU(1,1)/\mathbf{Z}_2$ is locally isomorphic to $SO(2,1)$. Indeed $SU(1,1)$ is a simply connected group and is the covering group of $SO(2,1)$.

$SO(3,1)$ has a covering space $SL(2, \mathbf{C})$ and we can write down relations among components of $SU(1,1)$ and $SL(2, \mathbf{C})$ by using a reduction of $SO(3,1)$ to $SO(2,1)$.

The group $SO(3,1)$ acts on a set of coordinates $x^\mu = (x^0, x^1, x^2, x^3)$ and x^μ transforms into $x'^\mu = \Lambda^\mu{}_\nu x^\nu$ ($\Lambda \in SO(3,1)$). By introducing the Pauli matrices, one can represent this transformation as a matrix form $\mathbf{x} = x^\mu \sigma_\mu$. The $SL(2, \mathbf{C})$ can act on this matrix as left/right multiplications by an element $\hat{g} \in SL(2, \mathbf{C})$.

$$x^\mu = (x^0, x^1, x^2, x^3), \quad \sigma_\mu = (1, \sigma_1, \sigma_2, \sigma_3), \tag{A.5}$$

$$\mathbf{x} := x^\mu \sigma_\mu = \begin{pmatrix} x^0 + x^3 & x^1 - ix^2 \\ x^1 + ix^2 & x^0 - x^3 \end{pmatrix}, \tag{A.6}$$

$$\hat{g} = \exp \left(i\vec{\theta} \cdot \frac{\vec{\sigma}}{2} - \vec{\omega} \cdot \frac{\vec{\sigma}}{2} \right), \quad \det \hat{g} = 1, \tag{A.7}$$

$$x'^\mu = \Lambda^\mu{}_\nu x^\nu, \quad \mathbf{x}' = \hat{g} \cdot \mathbf{x} \cdot \hat{g}^\dagger. \tag{A.8}$$

We can construct $SO(2,1)$ group by putting $x^3 = 0$ and restricting $SO(3,1)$ into $SO(2,1)$. Then the covering space $SL(2; \mathbf{C})$ is reduced to $SU(1,1)$. But one has to impose a constraint $\hat{g} \cdot \sigma_3 \cdot \hat{g}^\dagger = \sigma_3$ for $\hat{g} \in SL(2; \mathbf{C})$ to remove mixing between the x^3 part and the remaining 3-dimensional parts. This condition leads to a restriction of components of $\hat{g} \in SL(2; \mathbf{C})$ and induces an element of $g' \in SU(1,1)$, which is parameterized by two complex parameters a, b with a constraint $|a|^2 - |b|^2 = 1$,

$$SL(2; \mathbf{C}) \ni \hat{g} = \begin{pmatrix} a & b \\ c & d \end{pmatrix}, \quad ad - bc = 1, \quad a, b, c, d \in \mathbf{C}, \tag{A.9}$$

$$SU(1,1) \ni g' = \begin{pmatrix} a & b \\ \bar{b} & \bar{a} \end{pmatrix}, \quad |a|^2 - |b|^2 = 1, \quad a, b \in \mathbf{C}. \tag{A.10}$$

Every element $g' \in S(1,1)$ satisfies a constraint $g' \cdot \sigma_3 \cdot g'^\dagger = \sigma_3$. It induces a natural reduction of $SL(2; \mathbf{C})$ to $SU(1,1)$ associated with the reduction of $SO(3,1)$ to $SO(2,1)$.

Then we can write down the corresponding element $\Lambda^\mu{}_\nu$ of $SO(2, 1)$ as

$$SO(2, 1) \ni \Lambda^\mu{}_\nu = \begin{pmatrix} |a|^2 + |b|^2 & 2\text{Re}(a\bar{b}) & 2\text{Im}(a\bar{b}) \\ 2\text{Re}(ab) & \text{Re}(a^2 + b^2) & \text{Im}(a^2 - b^2) \\ -2\text{Im}(ab) & -\text{Im}(a^2 + b^2) & \text{Re}(a^2 - b^2) \end{pmatrix}, |a|^2 - |b|^2 = 1. \quad (\text{A.11})$$

By recalling the relations between $SU(1, 1)$ and $SL(2; \mathbf{R})$, we can show an element $g \in SL(2; \mathbf{R})$ in this parameterization as

$$SL(2; \mathbf{R}) \ni g = \begin{pmatrix} \text{Re}(a) + \text{Im}(b) & \text{Re}(b) + \text{Im}(a) \\ \text{Re}(b) - \text{Im}(a) & \text{Re}(a) - \text{Im}(b) \end{pmatrix}, |a|^2 - |b|^2 = 1. \quad (\text{A.12})$$

A.2 Representation of $su(1, 1)$

For the universal covering group associated with locally isomorphic Lie groups, all its irreducible representations are single-valued. Keeping this in our mind, we study representations of the Lie algebra $su(1, 1)$.

The Lie algebra $su(1, 1)$ is generated by a set of J_a 's ($a = 1, 2, 3$). The commutation relations are expressed in the form

$$[J_1, J_2] = -iJ_3, [J_2, J_3] = iJ_1, [J_3, J_1] = iJ_2, \quad (\text{A.13})$$

$$J_a^\dagger = J_a. \quad (\text{A.14})$$

By introducing J_\pm , we rewrite commutators of the generators as

$$J_\pm = J_1 \pm iJ_2, (J_\pm)^\dagger = J_\mp, \quad (\text{A.15})$$

$$[J_+, J_-] = -2J_3, [J_3, J_\pm] = \pm J_\pm, \quad (\text{A.16})$$

and a Casimir invariant is represented as a quadratic form

$$J^2 = J_1^2 + J_2^2 - J_3^2 = \frac{1}{2}(J_+J_- + J_-J_+) - J_3^2 = J_\pm J_\mp \pm J_3 - J_3^2. \quad (\text{A.17})$$

When we take a redefinition $L_0 = -J_3$, $L_{\pm 1} = J_\pm$, we can express the Lie algebra $sl(2, \mathbf{R})$ with generators L_n ($n = 0, \pm 1$). Their commutation relations are written as $[L_{+1}, L_{-1}] = 2L_0$, $[L_0, L_{\pm 1}] = \mp L_{\pm 1}$.

Now we shall consider representations of $su(1, 1)$. The operators J_3 and J^2 are hermitian operators and their eigenvalues are respectively real numbers $a \in \mathbf{R}$, $\Lambda \in \mathbf{R}$. The states of the Lie algebra are labelled by this set of eigenvalues (Λ, a) ,

$$J^2|\Lambda, a\rangle = \Lambda|\Lambda, a\rangle, J_3|\Lambda, a\rangle = a|\Lambda, a\rangle. \quad (\text{A.18})$$

By using $(J_\mp)^\dagger J_\mp = J_\pm J_\mp = J^2 + J_3^2 \mp J_3$, a useful condition is obtained as

$$J_\pm J_\mp |\Lambda, a\rangle = [\Lambda + a(a \mp 1)]|\Lambda, a\rangle, \quad (\text{A.19})$$

$$\Lambda + a(a \mp 1) \geq 0. \quad (\text{A.20})$$

Here we assumed the inner product is positive definite. It is the natural assumption in the unitary theories.

$\Lambda \leq 0$	$(j \geq 0)$	(A.24)
$0 < \Lambda \leq \frac{1}{4}$	$(-\frac{1}{2} \leq j < 0)$	
$0 \leq \Lambda < \frac{1}{4}$	$(-1 \leq j < -\frac{1}{2})$	
$\Lambda < 0$	$(j < -1)$	

Figure 8. The values of Λ and the range of j are shown in the table. Λ is negative or zero for the cases $j \geq 0$ or $j < -1$. On the other hand, Λ is positive but is less than or equal to $\frac{1}{4}$ for the case $-1 \leq j < 0$.

We can also show that the generator J_+ raises the eigenvalue a by one (when it satisfies $\langle \Lambda, a' | J_+ | \Lambda, a \rangle \neq 0$) by considering the following equation

$$\langle \Lambda, a' | J_+ | \Lambda, a \rangle = \langle \Lambda, a' | [J_3, J_+] | \Lambda, a \rangle = (a' - a) \langle \Lambda, a' | J_+ | \Lambda, a \rangle. \quad (\text{A.21})$$

By using these two properties, we study unitary representations of $su(1, 1)$. The representation is labelled by Λ of the Casimir invariant. We parameterise $\Lambda = -j(j+1)$ by $j \in \mathbf{C}$. The Casimir is the hermitian operator and its eigenvalue must be a real number. The reality of Λ leads to an important constraint that Λ is expressed in either of the following two series,

$$\Lambda \in \mathbf{R} \Rightarrow \begin{cases} j = \alpha \ (\alpha \in \mathbf{R}) \\ j = -\frac{1}{2} + i\beta \ (\beta \in \mathbf{R}). \end{cases} \quad (\text{A.22})$$

Each series is respectively parameterised by a set of real numbers, α and β . One can show only these two are possible by a direct calculation with $j = \alpha + i\beta$ ($\alpha, \beta \in \mathbf{R}$) as follows:

$$\begin{aligned} \Lambda &= -(\alpha + i\beta)[(\alpha + 1) + i\beta] \\ &= \{-\alpha(\alpha + 1) + \beta^2\} - i\beta(2\alpha + 1) \in \mathbf{R}. \end{aligned} \quad (\text{A.23})$$

In the first case $j \in \mathbf{R}$, the states are labelled by a set of real numbers (j, a) . Λ is also found to be less than or equal to $\frac{1}{4}$ from the relation $\Lambda = \frac{1}{4} - (j + \frac{1}{2})^2 \leq \frac{1}{4}$. There are four regions of j according to the value of Λ , as described in Fig. 8. However, $\Lambda = -j(j+1)$ is invariant under a transformation $j \rightarrow -j - 1$, so we can restrict j to be negative, $j < 0$. Then, in summary, the states are labelled by a set of real numbers (j, a) with $j < 0$.

In the second case $j = -\frac{1}{2} + i\beta$ ($0 \neq \beta \in \mathbf{R}$), a relation $\Lambda = \frac{1}{4} + \beta^2 > \frac{1}{4}$ is satisfied and Λ is greater than $\frac{1}{4}$. These two cases are complementary to each other in view of the values of Λ .

Next we turn to the states $|\Lambda, a\rangle$ in the first case and investigate properties of the states. The semi-positivity condition for the operator $J_{\pm}^{\dagger} J_{\pm}$, will give allowed regions in the (j, a) -plane. By recalling the equations,

$$J_+ J_- |\Lambda, a\rangle = (a - j - 1)(a + j) |\Lambda, a\rangle, \quad (\text{A.25})$$

$$J_- J_+ |\Lambda, a\rangle = (a + j + 1)(a - j) |\Lambda, a\rangle, \quad (\text{A.26})$$

we can write down constraints for (j, a) ,

$$0 \leq \Lambda + a(a \mp 1) = -j(j+1) + a(a \mp 1), \quad (\text{A.27})$$

$$(a-j-1)(a+j) \geq 0 \text{ and } (a+j+1)(a-j) \geq 0. \quad (\text{A.28})$$

By recalling $j < 0$, we have a condition $a \geq -j$ for a state $|\Lambda, a_0\rangle$. If $a > -j$ and $a \neq -j$ are satisfied, we will obtain non suitable states by acting J_- to the state $|\Lambda, a_0\rangle$ repeatedly. So we need a condition $a_0 = -j$ for an appropriate $a = a_0$ and obtain a discrete series of the states $D^+(j)$ which are constructed from $|\Lambda, a_0\rangle$ by applying J_+ repeatedly. The eigenvalues a 's of the states in this series are bounded from below and written as $a = a_0, a_0 + 1, a_0 + 2, \dots$.

As the second case, we have a discrete series $D^-(j)$ of the states by considering a condition $a < j$ ($j < 0$). The states in this series are labelled by a and j . In this series, the a 's take their values in discrete numbers $a = a_0, a_0 - 1, a_0 - 2, \dots$ which are bounded from above.

As the third case, we have continuous supplementary series $D_s(\Lambda, a_0)$. The states in this representation have eigenvalues a 's that take their values in discrete numbers $a = a_0, a_0 \pm 1, a_0 \pm 2, \dots$. They are neither bounded from above nor from below.

We have another continuous representation $D_p(\Lambda, a_0)$ labelled by a complex number $j = -\frac{1}{2} + i\beta$ ($\beta \in \mathbf{R}$) that is called as the continuous principal series. The states are characterised by the eigenvalues a 's and their values are written as $a = a_0, a_0 \pm 1, a_0 \pm 2, \dots$.

We summarize these four representations in the following. The allowed regions are illustrated by shaded regions in the Fig. 9. There are four types of representations. Three of them are associated to these regions in the Fig. 9. The remaining one corresponds to the case of the complex $j = -\frac{1}{2} + i\beta$ ($\beta \in \mathbf{R}$). The states are represented by $|\Lambda, a\rangle$ with $\Lambda = -j(j+1)$:

(a) Discrete series $D^+(j)$; bounded from below $\dots J_-|\Lambda, a_0\rangle = 0$

$$a_0 := -j \quad (j < 0) \quad (\text{A.29})$$

$$a = a_0, a_0 + 1, a_0 + 2, \dots \quad (\text{A.30})$$

(b) Discrete series $D^-(j)$; bounded from above $\dots J_+|\Lambda, a_0\rangle = 0$

$$a_0 := j \quad (j < 0) \quad (\text{A.31})$$

$$a = a_0, a_0 - 1, a_0 - 2, \dots \quad (\text{A.32})$$

(c) Continuous supplementary series $D_s(\Lambda, a_0)$; unbounded

$$\left| j + \frac{1}{2} \right| < \frac{1}{2} - |a_0|, \quad (\text{A.33})$$

$$a = a_0, a_0 \pm 1, a_0 \pm 2, \dots \quad (\text{A.34})$$

(d) Continuous principal series $D_p(\Lambda, a_0)$; unbounded

$$j = -\frac{1}{2} + i\beta \quad (\beta > 0) \quad (\text{A.35})$$

$$a = a_0, a_0 \pm 1, a_0 \pm 2, \dots \quad (\text{A.36})$$

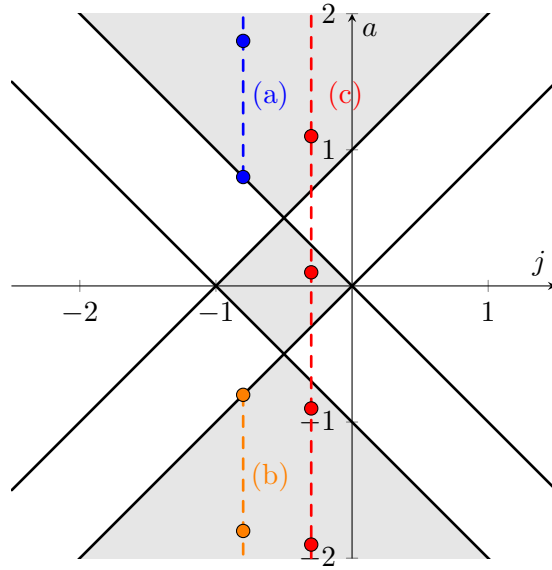


Figure 9. Representations of $su(1, 1)$. The allowed regions for a combination (j, a) are illustrated by shaded regions. The blue blobs belong to (a) discrete series bounded from below, the orange ones belong to (b) discrete series bounded from above, and the red ones belong to (c) continuous supplementary series which is unbounded.

B Solvable models and symmetry

In this appendix, we summarize the solvable models used in Sec. 4 and discuss their spectra from the viewpoint of the symmetry studied in App. A.

B.1 Inverted harmonic oscillator

B.1.1 $SL(2; \mathbf{R})$ symmetry and spectra

Using the representation theory described in Sec. A, we can obtain the spectra of a harmonic oscillator or an inverted harmonic oscillator. This is because the Hamiltonians of these systems in fact satisfy the algebra.

Let us consider a set of differential operators J_a 's ($a = 1, 2, 3$) as an example of a realization of this symmetry algebra $su(1, 1)$:

$$J_1 = \frac{1}{2} \left(\frac{d^2}{dx^2} + \frac{\tilde{a}}{x^2} + \frac{x^2}{4} \right), \quad (\text{B.1})$$

$$J_2 = \frac{-i}{2} \left(x \frac{d}{dx} + \frac{1}{2} \right), \quad (\text{B.2})$$

$$J_3 = \frac{1}{2} \left(\frac{d^2}{dx^2} + \frac{\tilde{a}}{x^2} - \frac{x^2}{4} \right), \quad (\text{B.3})$$

$$(J_a)^\dagger = J_a \quad (a = 1, 2, 3). \quad (\text{B.4})$$

The Casimir invariant is constant in this model, which is specified by the parameter \tilde{a} .

$$J^2 = J_1^2 + J_2^2 - J_3^2 = \frac{\tilde{a}}{4} + \frac{3}{16} = -j(j+1). \quad (\text{B.5})$$

Then j is expressed by using \tilde{a} as $j = -\frac{1}{2} \pm \frac{1}{2} \sqrt{\frac{1}{4} - \tilde{a}}$.

Now we shall study the hidden conformal symmetry proposed in [3] by using these differential operators with $\tilde{a} = 0$. We follow the notation of [3] and redefine the currents as

$$\hat{J}_3 = -iJ_1 = -\frac{i}{2} \left(\frac{d^2}{dx^2} + \frac{x^2}{4} \right) = \frac{i}{2} H, \quad (\text{B.6})$$

$$\hat{J}_1 = J_2 = -\frac{i}{2} \left(x \frac{d}{dx} + \frac{1}{2} \right), \quad (\text{B.7})$$

$$\hat{J}_2 = iJ_3 = \frac{i}{2} \left(\frac{d^2}{dx^2} - \frac{x^2}{4} \right) = -\frac{i}{2} H_{\text{ho}}, \quad (\text{B.8})$$

$$\hat{J}_{\pm} = \pm i \hat{J}_1 - \hat{J}_2 = \pm i J_2 - i J_3, \quad (\text{B.9})$$

$$[\hat{J}_+, \hat{J}_-] = -2\hat{J}_3, \quad [\hat{J}_3, \hat{J}_{\pm}] = \pm \hat{J}_{\pm}. \quad (\text{B.10})$$

This system is the inverted harmonic oscillator in 1 dimension with the Hamiltonian H . The spectrum of this model is represented as eigenvalues of $H = -2i\hat{J}_3$. In addition, the Casimir invariant is defined as

$$\hat{J}^2 = \hat{J}_3^2 - \hat{J}_1^2 - \hat{J}_2^2 = -J^2, \quad (\text{B.11})$$

$$\hat{J}^2 = \hat{J}_3^2 - \frac{1}{2}(\hat{J}_+ \hat{J}_- + \hat{J}_- \hat{J}_+) = \hat{J}_3^2 \pm \hat{J}_3 - \hat{J}_{\mp} \hat{J}_{\pm}, \quad (\text{B.12})$$

$$J^2 \cong \Lambda = -j(j+1), \quad (\text{B.13})$$

$$\hat{J}^2 \cong \hat{\Lambda} = -\Lambda = j(j+1) = \hat{j}(\hat{j}-1), \quad (\text{B.14})$$

$$\hat{j} := j+1. \quad (\text{B.15})$$

The states are labelled by a set of integers (\hat{j}, m) with

$$\hat{J}^2 \cong \hat{\Lambda} = \hat{j}(\hat{j}-1), \quad (\text{B.16})$$

$$\hat{J}_3 \cong m. \quad (\text{B.17})$$

By using the explicit form of the differential operators, one can obtain a relation

$$\hat{J}^2 = -\frac{3}{16}. \quad (\text{B.18})$$

It determines the values of \hat{j} as $\hat{j} = \frac{1}{4}, \frac{3}{4}$. We introduce a useful notation to label these two eigenvalues as

$$\hat{j}_{\alpha} = \frac{2\alpha-1}{4} \quad (\alpha = 1, 2), \quad (\text{B.19})$$

$$\hat{J}^2 \cong \hat{j}_{\alpha}(\hat{j}_{\alpha}-1), \quad (\text{B.20})$$

$$\hat{J}_3 \cong m. \quad (\text{B.21})$$

We can change the eigenvalue m by a unit by acting the raising \hat{J}_+ and the lowering \hat{J}_- operators on the state, to find

$$\hat{J}_{\mp} \hat{J}_{\pm} |\hat{j}, m\rangle = (m \pm \hat{j}) \{m \pm (1 - \hat{j})\} |\hat{j}, m\rangle$$

$$= (m \pm \frac{1}{4})(m \pm \frac{3}{4})|\hat{j}, m\rangle. \quad (\text{B.22})$$

Let us take the following two representations of this algebra and estimate the energy spectrum $H = -2i\hat{J}_3$.

1. Spectrum bounded from below

$$\hat{J}_-|\hat{j}_\alpha, m_0\rangle = 0 \cdots m_0 = +\hat{j}_\alpha, \quad (\text{B.23})$$

$$\hat{J}_+^k|\hat{j}_\alpha, +\hat{j}_\alpha\rangle \cdots H \cong -2i(k + \hat{j}_\alpha) = -i(n + \frac{1}{2}), \quad (\text{B.24})$$

$$n = 2k + \alpha - 1. \quad (\text{B.25})$$

2. Spectrum bounded from above

$$\hat{J}_+|\hat{j}_\alpha, m_0\rangle = 0 \cdots m_0 = -\hat{j}_\alpha, \quad (\text{B.26})$$

$$\hat{J}_-^k|\hat{j}_\alpha, -\hat{j}_\alpha\rangle \cdots H \cong -2i(-k - \hat{j}_\alpha) = +i(n + \frac{1}{2}), \quad (\text{B.27})$$

$$n = 2k + \alpha - 1. \quad (\text{B.28})$$

Then one can construct eigenstates $|n, \pm\rangle$ ($n = 0, 1, 2, \dots$) and associated eigenfunctions $\tilde{\Phi}_n^{(\pm)}(x)$ as

$$|n, \pm\rangle := \hat{J}_\pm^k|\hat{j}_\alpha, \pm\hat{j}_\alpha\rangle, \quad (\text{B.29})$$

$$n = 2k + \alpha - 1, \quad \hat{j}_\alpha = \frac{2\alpha - 1}{4} \quad (\alpha = 1, 2), \quad (\text{B.30})$$

$$\tilde{\Phi}_n^{(\pm)}(x) = \langle x|n, \pm\rangle, \quad (\text{B.31})$$

$$\tilde{\Phi}_{0,\alpha}^{(\pm)} = x^{\alpha-1} \cdot e^{\pm \frac{i}{4}x^2} \quad (\alpha = 1, 2), \quad (\text{B.32})$$

$$\tilde{\Phi}_{k,\alpha}^{(\pm)}(x) = e^{\pm \frac{i}{4}x^2} \cdot H_n \left(e^{\mp \frac{\pi i}{4}} \frac{x}{\sqrt{2}} \right), \quad (\text{B.33})$$

$$H_n(x) = (-1)^n e^{x^2} \left(\frac{d}{dx} \right)^n e^{-x^2}. \quad (\text{B.34})$$

This system is the inverted harmonic oscillator, and its spectra match the eigenvalues of the Schrödinger equation. We will see the details of the wave functions in Sec. B.1.2.

The spectra are also related to those of the usual harmonic oscillator by a change of variables: by considering a rotation in the 2,3-plane, we can transform the equation of the harmonic oscillator ($H_{\text{ho}}\tilde{\Phi}_{\text{ho}} = E_{\text{ho}}\tilde{\Phi}_{\text{ho}}$) into that of the inverted potential case ($H\tilde{\Phi} = E\tilde{\Phi}$), with $D_\pm := \exp\left[\pm \frac{\pi}{2}\hat{J}_1\right]$, as

$$D_\pm \cdot H \cdot D_\pm^{-1} = \pm iH_{\text{ho}}, \quad (\text{B.35})$$

$$\tilde{\Phi}(x) = D_\pm^{-1}\tilde{\Phi}_{\text{ho}}(x) = e^{\pm \frac{\pi i}{8}}\tilde{\Phi}_{\text{ho}}(e^{\pm \frac{\pi i}{4}}x), \quad (\text{B.36})$$

$$E = \pm iE_{\text{ho}}. \quad (\text{B.37})$$

B.1.2 Wave functions and spectra

Here let us turn to the Schrödinger equation of the inverted harmonic oscillator in one dimension, and look at the solutions to identify what kind of boundary conditions are implicitly imposed in the spectrum obtained by the symmetry argument in Sec. B.1.1.

The Schrödinger equation determines the energy eigenvalue E and the associated wavefunction $\psi(x)$

$$\left(\frac{d^2}{dx^2} + E + \frac{1}{4}x^2\right)\psi = 0. \quad (\text{B.38})$$

By changing variables $z := e^{\frac{\pi i}{4}} \cdot x$, $\nu := -\frac{1}{2} - iE$, one can rewrite this equation into a differential equation

$$\left(\frac{d^2}{dz^2} + \nu + \frac{1}{2} - \frac{1}{4}z^2\right)\psi = 0. \quad (\text{B.39})$$

This has two independent solutions expressed by the parabolic cylinder functions $D_\nu(z)$, $D_{-\nu-1}(iz)$ and $\psi(x)$ is described as a linear combination of them

$$\psi(z) = A \cdot D_\nu(z) + B \cdot D_{-\nu-1}(iz). \quad (\text{B.40})$$

We here summarize several useful formulas of the parabolic cylinder function. The function $D_\nu(z)$ is represented by the confluent hypergeometric function

$$D_\nu(z) = 2^{\frac{\nu}{2}}\sqrt{\pi} \cdot e^{-\frac{z^2}{4}} \left[\frac{1}{\Gamma(\frac{1-\nu}{2})} F\left(\frac{-\nu}{2}; \frac{1}{2}; \frac{z^2}{2}\right) - \frac{\sqrt{2}}{\Gamma(-\frac{\nu}{2})} z \cdot F\left(\frac{1-\nu}{2}; \frac{3}{2}; \frac{z^2}{2}\right) \right]. \quad (\text{B.41})$$

The differential equation (B.39) has four types of solutions $D_\nu(z)$, $D_{-\nu}(z)$, $D_{-\nu-1}(iz)$, and $D_{-\nu-1}(-iz)$. They are related one another by the following identities

$$D_\nu(z) = \frac{\Gamma(\nu+1)}{\sqrt{2\pi}} \left[e^{+\frac{\pi i}{2}\nu} D_{-\nu-1}(iz) + e^{-\frac{\pi i}{2}\nu} D_{-\nu-1}(-iz) \right], \quad (\text{B.42})$$

$$D_\nu(z) = e^{\pm\pi i\nu} D_\nu(-z) + \frac{\sqrt{2\pi}}{\Gamma(-\nu)} e^{\pm\frac{\pi i}{2}(\nu+1)} D_{-\nu-1}(\mp iz). \quad (\text{B.43})$$

The function $D_\nu(z)$ has an asymptotic form in the region $|z| \gg 1$ ($\nu \neq 0, 1, 2, \dots$) according to the argument of z ,

$$D_\nu(z) \sim e^{-\frac{z^2}{4}} z^\nu - \frac{\sqrt{2\pi}}{\Gamma(-\nu)} e^{+\nu\pi i} e^{+\frac{z^2}{4}} z^{-\nu-1} \quad \left(\frac{\pi}{4} < \arg z < \frac{5\pi}{4}\right), \quad (\text{B.44})$$

$$D_\nu(z) \sim e^{-\frac{z^2}{4}} z^\nu - \frac{\sqrt{2\pi}}{\Gamma(-\nu)} e^{-\nu\pi i} e^{+\frac{z^2}{4}} z^{-\nu-1} \quad \left(-\frac{5\pi}{4} < \arg z < -\frac{\pi}{4}\right), \quad (\text{B.45})$$

$$D_\nu(z) \sim e^{-\frac{z^2}{4}} z^\nu \quad \left(-\frac{3\pi}{4} < \arg z < \frac{3\pi}{4}\right). \quad (\text{B.46})$$

For $\nu = n \in \mathbf{Z}_{\geq 0}$, $D_\nu(z)$ is represented by the Hermite polynomial $H_n(z)$

$$D_n(z) = (-1)^n e^{\frac{z^2}{4}} \frac{d^n}{dz^n} e^{-\frac{z^2}{2}} = 2^{-\frac{n}{2}} e^{-\frac{z^2}{4}} H_n\left(\frac{z}{\sqrt{2}}\right), \quad (\text{B.47})$$

$$H_n(z) := (-1)^n e^{z^2} \frac{d^n}{dz^n} e^{-z^2}. \quad (\text{B.48})$$

When there is the inverted harmonic potential, the waves are scattered by this repulsive potential. In the region $x > 0$ ($z = e^{\frac{\pi i}{4}} \cdot x$), the wavefunction $\psi(x)$ behaves at $x \rightarrow +\infty$ as

$$\psi(z) \sim A \cdot e^{-\frac{z^2}{4}} \cdot z^\nu + B \cdot e^{+\frac{z^2}{4}} \cdot (iz)^{-\nu-1}. \quad (\text{B.49})$$

If the system time-evolves according to the factor $e^{-i\Omega t}$ in the wave function, one can see that the first term $e^{-\frac{z^2}{4}} = e^{-i\frac{x^2}{4}}$ is related to a left-moving wave (in-going mode as seen from the potential hill). On the other hand, the second term $e^{+\frac{z^2}{4}} = e^{+i\frac{x^2}{4}}$ represents a right-moving wave (in-going mode).

In order to analyze the scattering process, we want to know the behavior in the region $x \rightarrow -\infty$. The two solutions can be transformed by analytic continuations with $\tilde{x} := -x$ ($\tilde{x} > 0$)

$$\tilde{z} := e^{\frac{\pi i}{4}} \cdot \tilde{x}, \quad (\text{B.50})$$

$$\psi(z) = \psi(-\tilde{z}) = A \cdot D_\nu(-\tilde{z}) + B \cdot D_{-\nu-1}(-i\tilde{z}) \quad (\text{B.51})$$

$$= A' \cdot D_\nu(\tilde{z}) + B' \cdot D_{-\nu-1}(i\tilde{z}). \quad (\text{B.52})$$

Now we have two sets of coefficients (A, B) and (A', B') those encode the information of the scattering. There are relations between (A, B) and (A', B') :

$$\begin{pmatrix} A' \\ B' \end{pmatrix} = \begin{pmatrix} T_{11} & T_{12} \\ T_{21} & T_{22} \end{pmatrix} \begin{pmatrix} A \\ B \end{pmatrix}, \quad (\text{B.53})$$

$$T_{11} = e^{\pi i \nu}, \quad T_{21} = \frac{\sqrt{2\pi}}{\Gamma(-\nu)} e^{\frac{\pi i}{2}(\nu+1)}, \quad T_{12} = \frac{\sqrt{2\pi}}{\Gamma(\nu+1)} e^{\frac{\pi i}{2}\nu}, \quad T_{22} = e^{\pi i(\nu+1)}. \quad (\text{B.54})$$

In the region $x \rightarrow -\infty$, the first term $e^{-\frac{z^2}{4}} = e^{-i\frac{x^2}{4}}$ with A' is a right-moving wave (in-going mode), while the second term $e^{+\frac{z^2}{4}} = e^{+i\frac{x^2}{4}}$ with B' represents a left-moving wave (out-going mode).

The boundary conditions which one likes to impose for the wave functions are used for determining the coefficients (A, B) and (A', B') . To illustrate how the condition on the coefficients can determine the spectrum, let us consider quasinormal modes with the condition

$$A = A' = 0. \quad (\text{B.55})$$

This condition amounts to the boundary condition of having purely out-going modes on the both sides of the potential hill. We have an equation $T_{12} = \frac{\sqrt{2\pi}}{\Gamma(\nu+1)} e^{\frac{\pi i}{2}\nu} = 0$ from $A' = T_{11}A + T_{12}B = T_{12}B = 0$. The poles of $\Gamma(\nu+1)$ have contribution to this equation and we have a series of solutions

$$\nu = -n - 1 \quad (n = 0, 1, 2, \dots). \quad (\text{B.56})$$

In this discrete series, the associated wavefunction can be described by the Hermite polynomial

$$\psi(z) = B \cdot D_{-\nu-1}(iz) = B \cdot D_n(iz), \quad (\text{B.57})$$

$$D_n(z) = (-1)^n e^{\frac{z^2}{4}} \frac{d^n}{dz^n} e^{-\frac{z^2}{2}} = 2^{-\frac{n}{2}} \cdot e^{-\frac{z^2}{4}} H_n\left(\frac{z}{\sqrt{2}}\right), \quad (\text{B.58})$$

$$H_n(z) = (-1)^n e^{z^2} \frac{d^n}{dz^n} e^{-z^2}. \quad (\text{B.59})$$

Now we shall relate this spectral formula (B.56) to the quasinormal mode spectrum of the black hole. When one considers a wave equation of the scalar field Φ , the radial part $\psi(r)$ is described by the Schrödinger equation

$$\left(\frac{d^2}{dr_*^2} + \Omega^2 - V(r) \right) \psi = 0, \quad (\text{B.60})$$

$$V = V(r_{\text{PS}}) + \frac{1}{2} (f(r_{\text{PS}})^2 \cdot V''(r_{\text{PS}})) \cdot (\delta r_*)^2, \quad (\text{B.61})$$

$$\delta r_* = r_* - (r_*)_{\text{PS}}. \quad (\text{B.62})$$

When we associate x and E with δr_* and Ω , this system is reduced to the inverted harmonic oscillator

$$x = (-2 \cdot f(r_{\text{PS}})^2 \cdot V''(r_{\text{PS}}))^{1/4} \cdot \delta r_*, \quad (\text{B.63})$$

$$E = \frac{\Omega^2 - V(r_{\text{PS}})}{(-2 \cdot f(r_{\text{PS}})^2 \cdot V''(r_{\text{PS}}))^{1/2}}, \quad (\text{B.64})$$

$$\left(\frac{d^2}{dx^2} + E + \frac{1}{4} x^2 \right) \psi = 0. \quad (\text{B.65})$$

By recalling the above analysis, we can write down the values E and Ω^2 that are characterised by a set of integer n ($n = 0, 1, 2, \dots$)

$$E = i \left(\nu + \frac{1}{2} \right) = -i \left(n + \frac{1}{2} \right) \quad (n = 0, 1, 2, \dots), \quad (\text{B.66})$$

$$\Omega^2 = V(r_{\text{PS}}) + (-2 \cdot f(r_{\text{PS}})^2 \cdot V''(r_{\text{PS}}))^{1/2} \times E \quad (\text{B.67})$$

$$= V(r_{\text{PS}}) + 2\sqrt{V(r_{\text{PS}})} \cdot \gamma_L \times (-i) \left(n + \frac{1}{2} \right). \quad (\text{B.68})$$

If there is a condition $\frac{2\gamma_L}{\sqrt{V(r_{\text{PS}})}} \left(n + \frac{1}{2} \right) \ll 1$, we have a formula for the quasinormal mode spectrum Ω as

$$\Omega = \sqrt{V(r_{\text{PS}})} - i\gamma_L \cdot \left(n + \frac{1}{2} \right). \quad (\text{B.69})$$

In the case of the Schwarzschild black hole, one can estimate $\sqrt{V(r_{\text{PS}})} = \ell \frac{\sqrt{f(r_{\text{PS}})}}{r_{\text{PS}}}$, $\gamma_L = \frac{\sqrt{f(r_{\text{PS}})}}{r_{\text{PS}}}$. Then we obtain a restriction $\frac{2}{\ell} \times \left(n + \frac{1}{2} \right) \ll 1$. This is the spectrum obtained in [4], and we conclude that the spectrum generated by the symmetry amounts to the boundary condition of purely out-going modes on the both sides of the potential hill.

In our case of the AdS Schwarzschild black hole studied in this paper, the existence of the hard wall of the AdS boundary actually breaks the $SL(2; \mathbf{R})$ symmetry. This can be seen by one of the the symmetry generators (B.2) which is a scaling operator. A concrete choice of the position of the hard wall $x = L$ spoils this generator, that is why our quasinormal mode spectrum in the AdS Schwarzschild black hole does not follow the $SL(2; \mathbf{R})$ symmetry.

B.2 Pöschl-Teller model

We summarise properties of the Pöschl-Teller model and the related algebra studied in the paper [38].

B.2.1 Wave functions and spectra

The model is the integrable system in one dimension with a potential $V(x) = \frac{V_0}{\cosh^2 \alpha x}$, $V_0 = -\alpha^2 \lambda(\lambda - 1)$. The parameter $\alpha > 0$ characterises the width of the potential in the x -direction and λ specifies the height of the peak V_0 of the potential. In this paper, we consider the repulsive case with $V_0 > 0$ and study the scattering processes by the barrier generated by $V(x)$. The dynamics is described by a Hamiltonian H . The energy ω^2 and the eigenfunction $\psi(x)$ are determined by a Schrödinger equation

$$V = \frac{V_0}{\cosh^2 \alpha x}, \quad V_0 = -\alpha^2 \lambda(\lambda - 1), \quad (\text{B.70})$$

$$H = -\frac{d^2}{dx^2} + V(x), \quad (\text{B.71})$$

$$H\psi = \omega^2 \psi. \quad (\text{B.72})$$

The wavefunction is expressed as a linear combination of two independent solutions $f_{\pm}(x)$

$$\psi(x) = A \cdot f_+(x) + B \cdot f_-(x), \quad (\text{B.73})$$

$$f_+(x) = (e^{\alpha x})^{\frac{i\omega}{\alpha}} \times F\left(\lambda, 1 - \lambda; \frac{e^{\alpha x}}{e^{\alpha x} + e^{-\alpha x}}\right), \quad (\text{B.74})$$

$$f_-(x) = (e^{\alpha x} + e^{-\alpha x})^{\frac{i\omega}{\alpha}} \times F\left(\lambda - \frac{i\omega}{\alpha}, 1 - \lambda - \frac{i\omega}{\alpha}; \frac{e^{\alpha x}}{e^{\alpha x} + e^{-\alpha x}}\right). \quad (\text{B.75})$$

In the large negative region $x \rightarrow -\infty$, we can evaluate the asymptotic behavior of $\psi(x)$

$$f_+(x) \sim e^{i\omega x}, \quad f_-(x) \sim e^{-i\omega x}, \quad (\text{B.76})$$

$$\psi(x) \sim A e^{i\omega x} + B e^{-i\omega x}. \quad (\text{B.77})$$

In order to analyse the scattering, we want to know an asymptotic behavior of $\psi(x)$ in the large positive region $x \rightarrow +\infty$. The two solutions $f_{\pm}(x)$ can be rewritten by analytic continuations

$$f_+(x) = e^{+i\omega x} \cdot T_{11}(\omega) \times F\left(\lambda, 1 - \lambda; \frac{e^{-\alpha x}}{e^{\alpha x} + e^{-\alpha x}}\right)$$

$$+(e^{\alpha x} + e^{-\alpha x})^{-\frac{i\omega}{\alpha}} \cdot T_{21}(\omega) \times F\left(\lambda + \frac{i\omega}{\alpha}, 1 - \lambda + \frac{i\omega}{\alpha}; \frac{e^{-\alpha x}}{e^{\alpha x} + e^{-\alpha x}}\right), \quad (\text{B.78})$$

$$f_-(x) = e^{-i\omega x} \cdot T_{22}(\omega) \times F\left(\lambda, 1 - \lambda; \frac{e^{-\alpha x}}{e^{\alpha x} + e^{-\alpha x}}\right) \\ + (e^{\alpha x} + e^{-\alpha x})^{+\frac{i\omega}{\alpha}} \cdot T_{12}(\omega) \times F\left(\lambda - \frac{i\omega}{\alpha}, 1 - \lambda - \frac{i\omega}{\alpha}; \frac{e^{-\alpha x}}{e^{\alpha x} + e^{-\alpha x}}\right), \quad (\text{B.79})$$

where coefficients T_{11} , T_{12} , T_{21} , T_{22} are defined as

$$T_{11} = \frac{\Gamma(1 + \frac{i\omega}{\alpha})\Gamma(\frac{i\omega}{\alpha})}{\Gamma(1 - \lambda + \frac{i\omega}{\alpha})\Gamma(\lambda + \frac{i\omega}{\alpha})}, \quad (\text{B.80})$$

$$T_{21} = \frac{\Gamma(1 + \frac{i\omega}{\alpha})\Gamma(-\frac{i\omega}{\alpha})}{\Gamma(1 - \lambda)\Gamma(\lambda)}, \quad (\text{B.81})$$

$$T_{12} = \frac{\Gamma(1 - \frac{i\omega}{\alpha})\Gamma(\frac{i\omega}{\alpha})}{\Gamma(1 - \lambda)\Gamma(\lambda)}, \quad (\text{B.82})$$

$$T_{22} = \frac{\Gamma(1 - \frac{i\omega}{\alpha})\Gamma(-\frac{i\omega}{\alpha})}{\Gamma(1 - \lambda - \frac{i\omega}{\alpha})\Gamma(\lambda - \frac{i\omega}{\alpha})}. \quad (\text{B.83})$$

In the region $x \rightarrow +\infty$, the wavefunction $\psi(x)$ behaves as

$$f_+(x) \sim T_{11}(\omega)e^{i\omega x} + T_{21}(\omega)e^{-i\omega x}, \quad (\text{B.84})$$

$$f_-(x) \sim T_{12}(\omega)e^{i\omega x} + T_{22}(\omega)e^{-i\omega x}, \quad (\text{B.85})$$

$$\psi(x) \sim A'e^{i\omega x} + B'e^{-i\omega x}, \quad (\text{B.86})$$

where A' , B' are related to A , B by equations

$$\begin{pmatrix} A' \\ B' \end{pmatrix} = \begin{pmatrix} T_{11} & T_{12} \\ T_{21} & T_{22} \end{pmatrix} \begin{pmatrix} A \\ B \end{pmatrix}. \quad (\text{B.87})$$

When we take the point $x = 0$ as a reference point of the scattering, the waves with coefficients A , B' are in-going ones. On the otherhand, B and A' counterparts are out-going waves. As boundary conditions, we put $A = B' = 0$ and obtain a relation $T_{22}(\omega) = \frac{\Gamma(1 - \frac{i\omega}{\alpha})\Gamma(-\frac{i\omega}{\alpha})}{\Gamma(1 - \lambda - \frac{i\omega}{\alpha})\Gamma(\lambda - \frac{i\omega}{\alpha})} = 0$. The gamma functions in the denominator have poles in the ω -plane and they determine quasinormal modes $\omega_n^{(\pm)}$ ($n = 0, 1, 2, \dots$)

$$\omega_n^{(\pm)} = -i\alpha \left(n + \lambda^{(\pm)} \right), \quad (n = 0, 1, 2, \dots) \quad (\text{B.88})$$

$$\lambda^{(+)} := \lambda, \quad \lambda^{(-)} := 1 - \lambda. \quad (\text{B.89})$$

In this case, the wavefunction $\psi(x) = B \cdot \psi_n^{(\pm)}(x)$ is written by the hypergeometric function

$$\psi_n^{(\pm)}(x) = (e^{\alpha x} + e^{-\alpha x})^{\frac{i\omega_n^{(\pm)}}{\alpha}} \\ \times F\left(\lambda - \frac{i\omega_n^{(\pm)}}{\alpha}, 1 - \lambda - \frac{i\omega_n^{(\pm)}}{\alpha}; \frac{e^{\alpha x}}{e^{\alpha x} + e^{-\alpha x}}\right)$$

$$\begin{aligned}
&= (e^{\alpha x} + e^{-\alpha x})^{n+\lambda^{(\pm)}} \\
&\times F\left(\begin{matrix} -n, 1 - 2\lambda^{(\pm)} - n \\ 1 - \lambda^{(\pm)} - n \end{matrix}; \frac{e^{\alpha x}}{e^{\alpha x} + e^{-\alpha x}}\right). \tag{B.90}
\end{aligned}$$

Now we will put $\lambda = \frac{1}{2} + i\nu$ ($\nu \in \mathbf{R}$) to reduce this potential model to the quasinormal modes of the black hole. It is the high barrier case and is related to the continuous representation of the Lie algebra $sl(2; \mathbf{R})$. In that case, the peak of $V(x)$ is $V_0 = \alpha^2(\frac{1}{4} + \nu^2)$ which is labelled by $\nu \in \mathbf{R}$ and the modes $\omega_n^{(\pm)}$'s are labelled by ν

$$\omega_n^{(\pm)} = -i\alpha \left(n + \frac{1}{2} \right) \pm \alpha\nu. \tag{B.91}$$

The wave propagates on the x -direction according to $e^{-i\omega t}$. The amplitude decreases exponentially $e^{-i\omega_n^{(\pm)}t} = e^{-\alpha(n+\frac{1}{2})t} e^{\mp i\alpha\nu t}$ with $\alpha = \gamma_L$. The parameter α is related to the Lyapunov exponent γ_L and specifies the time scale of the relaxation in the system.

The associated wavefunctions are also expressed by the Jacobi polynomial

$$y = \tanh \alpha x, \tag{B.92}$$

$$\begin{aligned}
\psi_n^{(\pm)}(x) &= (2 \cosh \alpha x)^{n+\frac{1}{2}\pm i\nu} \times F\left(\begin{matrix} -n, -n \mp 2i\nu \\ -n + \frac{1}{2} \mp i\nu \end{matrix}; \frac{1+y}{2}\right), \\
&F\left(\begin{matrix} -n, -n \mp 2i\nu \\ -n + \frac{1}{2} \mp i\nu \end{matrix}; \frac{1+y}{2}\right) \\
&= \left\{ \frac{(-1)^n}{n!} \frac{\Gamma(\mp i\nu + \frac{1}{2})}{\Gamma(\mp i\nu + \frac{1}{2} - n)} \right\}^{-1} \times P_n^{(\mp i\nu - \frac{1}{2} - n, \mp i\nu - \frac{1}{2} - n)}(y), \\
&P_n^{(\mp i\nu - \frac{1}{2} - n, \mp i\nu - \frac{1}{2} - n)}(y) \\
&= \frac{(-1)^n}{2^n \cdot n!} (1 - y^2)^{n+\frac{1}{2}\pm i\nu} \left(\frac{d}{dy} \right)^n (1 - y^2)^{-\frac{1}{2}\mp i\nu}. \tag{B.93}
\end{aligned}$$

We shall summarize useful relations for these functions

$$\begin{aligned}
P_n^{(\alpha, \beta)}(x) &= \frac{(-1)^n}{2^n \cdot n!} (1-x)^{-\alpha} (1+x)^{-\beta} \left(\frac{d}{dx} \right)^n [(1-x)^{\alpha+n} (1+x)^{\beta+n}], \\
P_n^{(\alpha, \beta)}(x) &= \frac{(-1)^n}{n!} \frac{\Gamma(n+1+\beta)}{\Gamma(1+\beta)} \times F\left(\begin{matrix} -n, n + \alpha + \beta + 1 \\ 1 + \beta \end{matrix}; \frac{1+x}{2}\right) \\
&= \frac{1}{n!} \frac{\Gamma(n+1+\alpha)}{\Gamma(1+\alpha)} \times F\left(\begin{matrix} -n, n + \alpha + \beta + 1 \\ 1 + \alpha \end{matrix}; \frac{1-x}{2}\right). \tag{B.94}
\end{aligned}$$

We also collect several properties of the hypergeometric functions here: The hypergeometric equation is defined as

$$z(1-z) \frac{d^2 f}{dz^2} + [c - (a+b+1)z] \frac{df}{dz} - abf = 0. \tag{B.95}$$

There is a set of solutions analytic around a point $z = 0$

$$f = F\left(\begin{matrix} a, b \\ c \end{matrix}; z\right), \tag{B.96}$$

$$f = z^{1-c} \cdot F \left(\begin{matrix} a-c+1, b-c+1 \\ 2-c \end{matrix}; z \right). \quad (\text{B.97})$$

They are suitable linearly independent solutions that converge under conditions $|z| < 1$, $\text{Re}(a+b-c) < 0$.

One can reexpress the hypergeometric function defined around $z = 0$ in terms of analytic functions around $z = 1$ through an analytic continuation,

$$\begin{aligned} F \left(\begin{matrix} a, b \\ c \end{matrix}; z \right) &= \frac{\Gamma(c)\Gamma(a+b-c)}{\Gamma(a)\Gamma(b)} (1-z)^{c-a-b} \times F \left(\begin{matrix} c-a, c-b \\ c-a-b+1 \end{matrix}; 1-z \right) \\ &+ \frac{\Gamma(c)\Gamma(c-a-b)}{\Gamma(c-a)\Gamma(c-b)} \times F \left(\begin{matrix} a, b \\ a+b-c+1 \end{matrix}; 1-z \right), \end{aligned} \quad (\text{B.98})$$

$|\arg(1-z)| < \pi.$

B.2.2 $SL(2; \mathbf{R})$ symmetry and spectra

The Pöschl-Teller model can be solved by the Jacobi polynomials in the high barrier case. We will discuss the symmetry of this model proposed in [38] in view of the Schrödinger equations. Our notation is different from that of [38]. By introducing a variable $y = \alpha x$, we rewrite the Hamiltonian as

$$H = -\frac{d^2}{dy^2} + V(y), \quad V(y) = -\frac{\lambda(\lambda-1)}{\cosh^2 y}, \quad (\text{B.99})$$

$$H\psi = \frac{\omega^2}{\alpha^2} \psi, \quad (\text{B.100})$$

and use a new parameter K_n defined as

$$K_n = \frac{i}{\alpha} \omega_n^{(\pm)} = \begin{cases} n + \lambda & (+) \text{ case} \\ n + 1 - \lambda & (-) \text{ case} \end{cases} \quad (n = 0, 1, 2, \dots).$$

From now on, we abbreviate the superscripts (\pm) and introduce a set of operators J^\pm, J^3 that act on the solutions $\{\psi_n\}$ ($n = 0, 1, 2, \dots$)

$$J_n^-; \psi_n \rightarrow \psi_{n-1}, \quad J_{n+1}^+; \psi_n \rightarrow \psi_{n+1}, \quad (\text{B.101})$$

$$J_n^3; \psi_n \rightarrow \psi_n, \quad (\text{B.102})$$

$$J_n^- = i(-\cosh y \partial_y + K_n \sinh y), \quad (\text{B.103})$$

$$J_{n+1}^+ = i(\cosh y \partial_y + K_n \sinh y), \quad (\text{B.104})$$

$$J_n^3 \psi_n = K_n \psi_n. \quad (\text{B.105})$$

These currents have been considered in solvable quantum mechanical models in one dimension. Here we use the convention in the paper [38]. But our convention is slightly different from that of the paper.

When the operators act on the set of solutions $\{\psi_n\}$, one can show the operators satisfy commutation relations that represent $su(1, 1)$ algebra

$$[J^3, J^\pm] = \pm J^\pm, \quad [J^+, J^-] = -2J^3. \quad (\text{B.106})$$

These are obtained from the following calculation

$$J_n^3 J_n^3 \psi_n = K_n^2 \psi_n, \quad (\text{B.107})$$

$$J_n^+ J_n^- \psi_n = \cosh^2 y \cdot \partial_y^2 \psi_n - K_n (1 + K_n \sinh^2 y) \cdot \psi_n, \quad (\text{B.108})$$

$$J_{n+1}^- J_{n+1}^+ \psi_n = \cosh^2 y \cdot \partial_y^2 \psi_n - K_n (-1 + K_n \sinh^2 y) \cdot \psi_n, \quad (\text{B.109})$$

$$J_{n-1}^3 J_n^- \psi_n = K_{n-1} J_n^- \psi_n, \quad (\text{B.110})$$

$$J_n^- J_n^3 \psi_n = K_n J_n^- \psi_n, \quad (\text{B.111})$$

$$J_{n+1}^3 J_{n+1}^+ \psi_n = K_{n+1} J_{n+1}^+ \psi_n, \quad (\text{B.112})$$

$$J_{n+1}^+ J_n^3 \psi_n = K_n J_{n+1}^+ \psi_n. \quad (\text{B.113})$$

Next we rewrite the Schrödinger equation

$$\left[\frac{d^2}{dy^2} - K_n^2 + \frac{\lambda(\lambda-1)}{\cosh^2 y} \right] \psi_n = 0 \quad (\text{B.114})$$

into the form

$$\cosh^2 y \cdot \partial_y^2 \psi_n = K_n^2 \cosh^2 y \cdot \psi_n - \lambda(\lambda-1) \psi_n, \quad (\text{B.115})$$

and evaluate the bilinears of the generators

$$J_n^3 J_n^3 \psi_n = K_n^2 \psi_n, \quad (\text{B.116})$$

$$\begin{aligned} -J_n^+ J_n^- \psi_n - J_{n+1}^- J_{n+1}^+ \psi_n \\ = -2 \cosh^2 y \cdot \partial_y^2 \psi_n + 2K_n^2 \sinh^2 y \cdot \psi_n \end{aligned} \quad (\text{B.117})$$

$$= -2[K_n^2 \cosh^2 y \cdot \psi_n - \lambda(\lambda-1) \psi_n] + 2K_n^2 \sinh^2 y \cdot \psi_n \quad (\text{B.118})$$

$$= -2K_n^2 \psi_n + 2\lambda(\lambda-1) \psi_n, \quad (\text{B.119})$$

to obtain

$$(-J^+ J^- - J^- J^+ + 2J^3 J^3) \psi_n = 2\lambda(\lambda-1) \psi_n. \quad (\text{B.120})$$

Then one can write down the Casimir invariant J^2 in this model by using the generators

$$J^2 = -J^3 J^3 + \frac{1}{2}(J^+ J^- + J^- J^+) = -\lambda(\lambda-1). \quad (\text{B.121})$$

The representation $su(1,1)$ is classified in terms of the eigenvalue of J^2 . It is related to the height V_0 of the peak of $V(x)$ and we can write down the V_0 in terms of the Casimir J^2

$$V_0 = -\alpha^2 \lambda(\lambda-1) = \alpha^2 J^2. \quad (\text{B.122})$$

We make a remark here: the Casimir J^2 is the hermitian operator and its eigenvalue is real number. But the generator J^3 is not hermitian and its eigenvalue K_n can take its value in complex number $n + \frac{1}{2} \pm i\nu$ ($\nu \in \mathbf{R}$), namely, the representation could be non-unitary.

References

- [1] J. M. Maldacena, “The Large N limit of superconformal field theories and supergravity,” *Adv. Theor. Math. Phys.* **2** (1998) 231–252, [arXiv:hep-th/9711200](#).
- [2] **Event Horizon Telescope** Collaboration, K. Akiyama *et al.*, “First M87 Event Horizon Telescope Results. I. The Shadow of the Supermassive Black Hole,” *Astrophys. J. Lett.* **875** (2019) L1, [arXiv:1906.11238](#) [[astro-ph.GA](#)].
- [3] B. Raffaelli, “Hidden conformal symmetry on the black hole photon sphere,” *JHEP* **03** (2022) 125, [arXiv:2112.12543](#) [[gr-qc](#)].
- [4] S. Hadar, D. Kapec, A. Lupsasca, and A. Strominger, “Holography of the photon ring,” *Class. Quant. Grav.* **39** no. 21, (2022) 215001, [arXiv:2205.05064](#) [[gr-qc](#)].
- [5] D. Kapec, A. Lupsasca, and A. Strominger, “Photon rings around warped black holes,” *Class. Quant. Grav.* **40** no. 9, (2023) 095006, [arXiv:2211.01674](#) [[gr-qc](#)].
- [6] Y. Chen, W. Guo, K. Shi, and H. Zhang, “ $SL(2, R) \times U(1)$ symmetry and quasinormal modes in the self-dual warped AdS black hole,” [arXiv:2303.11714](#) [[hep-th](#)].
- [7] B. Chen, Y. Hou, and Z. Hu, “On emergent conformal symmetry near the photon ring,” *JHEP* **05** (2023) 115, [arXiv:2212.02958](#) [[hep-th](#)].
- [8] K. Fransen, “Quasinormal Modes from Penrose Limits,” [arXiv:2301.06999](#) [[gr-qc](#)].
- [9] J. S. F. Chan and R. B. Mann, “Scalar wave falloff in asymptotically anti-de Sitter backgrounds,” *Phys. Rev. D* **55** (1997) 7546–7562, [arXiv:gr-qc/9612026](#).
- [10] G. T. Horowitz and V. E. Hubeny, “Quasinormal modes of AdS black holes and the approach to thermal equilibrium,” *Phys. Rev. D* **62** (2000) 024027, [arXiv:hep-th/9909056](#).
- [11] S. Kalyana Rama and B. Sathiapalan, “On the role of chaos in the AdS / CFT connection,” *Mod. Phys. Lett. A* **14** (1999) 2635–2648, [arXiv:hep-th/9905219](#).
- [12] G. Festuccia and H. Liu, “A Bohr-Sommerfeld quantization formula for quasinormal frequencies of AdS black holes,” *Adv. Sci. Lett.* **2** (2009) 221–235, [arXiv:0811.1033](#) [[gr-qc](#)].
- [13] V. Cardoso and J. P. S. Lemos, “Quasinormal modes of Schwarzschild anti-de Sitter black holes: Electromagnetic and gravitational perturbations,” *Phys. Rev. D* **64** (2001) 084017, [arXiv:gr-qc/0105103](#).
- [14] I. G. Moss and J. P. Norman, “Gravitational quasinormal modes for anti-de Sitter black holes,” *Class. Quant. Grav.* **19** (2002) 2323–2332, [arXiv:gr-qc/0201016](#).
- [15] A. O. Starinets, “Quasinormal modes of near extremal black branes,” *Phys. Rev. D* **66** (2002) 124013, [arXiv:hep-th/0207133](#).
- [16] R. A. Konoplya, “On quasinormal modes of small Schwarzschild-anti-de Sitter black hole,” *Phys. Rev. D* **66** (2002) 044009, [arXiv:hep-th/0205142](#).
- [17] G. Michalogiorgakis and S. S. Pufu, “Low-lying gravitational modes in the scalar sector of the global AdS(4) black hole,” *JHEP* **02** (2007) 023, [arXiv:hep-th/0612065](#).
- [18] G. Siopsis, “Low frequency quasi-normal modes of AdS black holes,” *JHEP* **05** (2007) 042, [arXiv:hep-th/0702079](#).

- [19] A. S. Miranda, J. Morgan, and V. T. Zanchin, “Quasinormal modes of plane-symmetric black holes according to the AdS/CFT correspondence,” *JHEP* **2008** no. 11, (2008) 030, [arXiv:0809.0297 \[hep-th\]](#).
- [20] V. Cardoso, A. S. Miranda, E. Berti, H. Witek, and V. T. Zanchin, “Geodesic stability, Lyapunov exponents and quasinormal modes,” *Phys. Rev. D* **79** no. 6, (2009) 064016, [arXiv:0812.1806 \[hep-th\]](#).
- [21] R. G. Daghigh and M. D. Green, “Highly Real, Highly Damped, and Other Asymptotic Quasinormal Modes of Schwarzschild-Anti De Sitter Black Holes,” *Class. Quant. Grav.* **26** (2009) 125017, [arXiv:0808.1596 \[gr-qc\]](#).
- [22] A. S. Miranda, C. A. Ballon Bayona, H. Boschi-Filho, and N. R. F. Braga, “Black-hole quasinormal modes and scalar glueballs in a finite-temperature AdS/QCD model,” *JHEP* **2009** no. 11, (2009) 119, [arXiv:0909.1790 \[hep-th\]](#).
- [23] E. Berti, V. Cardoso, and P. Pani, “Breit-Wigner resonances and the quasinormal modes of anti-de Sitter black holes,” *Phys. Rev. D* **79** (2009) 101501, [arXiv:0903.5311 \[gr-qc\]](#).
- [24] F. Denef, S. A. Hartnoll, and S. Sachdev, “Black hole determinants and quasinormal modes,” *Class. Quant. Grav.* **27** (2010) 125001, [arXiv:0908.2657 \[hep-th\]](#).
- [25] J. Morgan, V. Cardoso, A. S. Miranda, C. Molina, and V. T. Zanchin, “Gravitational quasinormal modes of AdS black branes in d spacetime dimensions,” *JHEP* **2009** no. 09, (2009) 117, [arXiv:0907.5011 \[hep-th\]](#).
- [26] J. Morgan, V. Cardoso, A. S. Miranda, C. Molina, and V. T. Zanchin, “Quasinormal modes of black holes in anti-de Sitter space: A Numerical study of the eikonal limit,” *Phys. Rev. D* **80** no. 2, (2009) 024024, [arXiv:0906.0064 \[hep-th\]](#).
- [27] R. G. Daghigh, “The Highly Real Quasinormal Modes of Schwarzschild-Anti De Sitter Black Holes,” *JHEP* **04** (2009) 045, [arXiv:0901.2353 \[gr-qc\]](#).
- [28] O. Gannot, “Quasinormal Modes for Schwarzschild-AdS Black Holes: Exponential Convergence to the Real Axis,” *Commun. Math. Phys.* **330** (2014) 771–799, [arXiv:1212.1907 \[math.SP\]](#).
- [29] A. Aragón, P. A. González, E. Papantonopoulos, and Y. Vásquez, “Anomalous decay rate of quasinormal modes in Schwarzschild-dS and Schwarzschild-AdS black holes,” *JHEP* **08** (2020) 120, [arXiv:2004.09386 \[gr-qc\]](#).
- [30] R. G. Daghigh, M. D. Green, and J. C. Morey, “Calculating quasinormal modes of Schwarzschild anti-de Sitter black holes using the continued fraction method,” *Phys. Rev. D* **107** no. 2, (2023) 024023, [arXiv:2209.09324 \[gr-qc\]](#).
- [31] S. Fortuna and I. Vega, “Electromagnetic quasinormal modes of Schwarzschild–anti–de Sitter black holes: Bifurcations, spectral similarity, and exact solutions in the large black hole limit,” *Phys. Rev. D* **106** no. 8, (2022) 084028, [arXiv:2202.12196 \[gr-qc\]](#).
- [32] E. Berti, V. Cardoso, and A. O. Starinets, “Quasinormal modes of black holes and black branes,” *Class. Quant. Grav.* **26** (2009) 163001, [arXiv:0905.2975 \[gr-qc\]](#).
- [33] R. A. Konoplya and A. Zhidenko, “Quasinormal modes of black holes: From astrophysics to string theory,” *Rev. Mod. Phys.* **83** (2011) 793–836, [arXiv:1102.4014 \[gr-qc\]](#).
- [34] K. Hashimoto, S. Kinoshita, and K. Murata, “Imaging black holes through the AdS/CFT correspondence,” *Phys. Rev. D* **101** no. 6, (2020) 066018, [arXiv:1811.12617 \[hep-th\]](#).

- [35] K. Hashimoto, S. Kinoshita, and K. Murata, “Einstein Rings in Holography,” *Phys. Rev. Lett.* **123** no. 3, (2019) 031602, [arXiv:1906.09113 \[hep-th\]](#).
- [36] V. Ferrari and B. Mashhoon, “Oscillations of a Black Hole,” *Phys. Rev. Lett.* **52** no. 16, (1984) 1361.
- [37] F. J. Zerilli, “Gravitational field of a particle falling in a schwarzschild geometry analyzed in tensor harmonics,” *Phys. Rev. D* **2** (1970) 2141–2160.
- [38] D. Çevik, M. Gadella, Ş. Kuru, and J. Negro, “Resonances and antibound states for the Pöschl–Teller potential: Ladder operators and SUSY partners,” *Phys. Lett. A* **380** (2016) 1600–1609, [arXiv:1601.05134 \[math-ph\]](#).
- [39] D. E. Berenstein, J. M. Maldacena, and H. S. Nastase, “Strings in flat space and pp waves from N=4 superYang-Mills,” *JHEP* **04** (2002) 013, [arXiv:hep-th/0202021](#).
- [40] A. Almheiri, T. Hartman, J. Maldacena, E. Shaghoulian, and A. Tajdini, “Replica Wormholes and the Entropy of Hawking Radiation,” *JHEP* **05** (2020) 013, [arXiv:1911.12333 \[hep-th\]](#).
- [41] Y. Kaku, K. Murata, and J. Tsujimura, “Observing black holes through superconductors,” *JHEP* **09** (2021) 138, [arXiv:2106.00304 \[hep-th\]](#).
- [42] Y. Liu, Q. Chen, X.-X. Zeng, H. Zhang, W.-L. Zhang, and W. Zhang, “Holographic Einstein ring of a charged AdS black hole,” *JHEP* **10** (2022) 189, [arXiv:2201.03161 \[hep-th\]](#).
- [43] Y. Kaku, K. Murata, and J. Tsujimura, “Creating stars orbiting in AdS,” *Phys. Rev. D* **106** no. 2, (2022) 026002, [arXiv:2202.07807 \[hep-th\]](#).
- [44] K. Hashimoto, Y. Matsuo, and T. Yoda, “String is a double slit,” *PTEP* **2023** no. 4, (2023) 043B04, [arXiv:2206.10951 \[hep-th\]](#).
- [45] S. Mandal, S. Upadhyay, Y. Myrzakulov, and G. Yergaliyeva, “Shadow of the 5D Reissner-Nordström AdS Black Hole,” [arXiv:2207.10085 \[gr-qc\]](#).
- [46] S. Caron-Huot, “Holographic cameras: an eye for the bulk,” *JHEP* **03** (2023) 047, [arXiv:2211.11791 \[hep-th\]](#).
- [47] K. Hashimoto, D. Takeda, K. Tanaka, and S. Yonezawa, “Spacetime-emergent ring toward tabletop quantum gravity experiments,” *Phys. Rev. Res.* **5** no. 2, (2023) 023168, [arXiv:2211.13863 \[hep-th\]](#).
- [48] X.-X. Zeng, K.-J. He, and G.-p. Li, “Holographic Einstein rings of a Gauss-Bonnet AdS black hole,” [arXiv:2302.03692 \[gr-qc\]](#).
- [49] S. Kinoshita, K. Murata, and D. Takeda, “Shooting null geodesics into holographic spacetimes,” [arXiv:2304.01936 \[hep-th\]](#).
- [50] J. Maldacena, S. H. Shenker, and D. Stanford, “A bound on chaos,” *JHEP* **08** (2016) 106, [arXiv:1503.01409 \[hep-th\]](#).
- [51] S. H. Shenker and D. Stanford, “Black holes and the butterfly effect,” *JHEP* **03** (2014) 067, [arXiv:1306.0622 \[hep-th\]](#).
- [52] J. Engelsöy, T. G. Mertens, and H. Verlinde, “An investigation of AdS₂ backreaction and holography,” *JHEP* **07** (2016) 139, [arXiv:1606.03438 \[hep-th\]](#).
- [53] K. Hashimoto and N. Tanahashi, “Universality in Chaos of Particle Motion near Black Hole Horizon,” *Phys. Rev. D* **95** no. 2, (2017) 024007, [arXiv:1610.06070 \[hep-th\]](#).

- [54] P. Bizon and A. Rostworowski, “On weakly turbulent instability of anti-de Sitter space,” *Phys. Rev. Lett.* **107** (2011) 031102, [arXiv:1104.3702 \[gr-qc\]](#).